Supplementary Material for

Phylogenomics of scorpions reveal contemporaneous diversification of scorpion mammalian predators and mammal-active sodium channel toxins

*Carlos E. Santibáñez-López, Shlomi Aharon, Jesús A. Ballesteros, Guilherme Gainett, Caitlin M. Baker, Edmundo González-Santillán, Mark S. Harvey, Mohamed K. Hassan, Ali Hussin Abu-Almaaty, Shorouk Mohamed Aldeyarbi, Lionel Monod, Andrés Ojanguren-Affilastro, Ricardo Pinto-da-Rocha, Yoram Zvik, Efrat Gavish-Regev, Prashant P. Sharma

* Correspondence to be sent to: Department of Biology, Western Connecticut State University, 181 White Street, Danbury, CT 06810, USA; E-mail: santibanezlopezc@wcsu.edu.

This PDF file includes:

SUPPLEMENTARY TEXT

Taxon sampling

Sequences from 100 species of Scorpiones were used for this study, of which 56 were sequenced previously by our team and 43 were newly sequenced for this study. In addition, transcriptomes of 20 outgroup taxa representing seven chelicerate orders were included. A full list of sequences, with taxonomic information, sources of previously published sequenced, and GenBank accession numbers, is provided in Supplementary Tables S1-3.

RNA extraction and sequencing

All specimens were either collected in the field with the aid of UV illumination, or from captive bred colonies (Table S2). From all specimens, the brain, legs and telson were dissected for sequencing, as in our previous publications (Santibáñez-López et al. 2019). For surveying transcriptional activity of venom gland tissue, scorpion venom glands were drained using a Parafilm membrane stretched across a 35-mm Petri dish target. All tissues were dissected into RNAlater solution (Ambion, Foster City, CA, USA). Total RNA extraction with TriZOL Trireagent (Ambion Life Technologies, Waltham, MA, USA), mRNA purification, and cDNA library construction using Illumina Tru-Seq kits were performed using manufacturers' protocols, as detailed in our recent works (Sharma et al. 2014; 2015; Santibáñez-López et al. 2018a; 2018b). Library preparation and stranded mRNA sequencing was performed at the Biotechnology Center at the University of Wisconsin-Madison or using an Apollo

324 automated system using the PrepX mRNA kit (IntegenX, Pleasanton, CA, USA) at Harvard University's Bauer Core Facility, with samples marked with unique indices to enable multiplexing. Samples were run using the Illumina HiSeq 2500 platform with paired-end reads of 100 or 150 bp at the FAS Center for Systems Biology at Harvard University, and using an Illumina HiSeq 2500 High Throughput platform with paired-end reads of 125-150 bp at the Biotechnology Center at the University of Wisconsin-Madison.

De novo transcriptome assemblies and orthology inference

Newly generated transcriptomes were assembled using Trinity v.2.5 (Trinity --seqType fq --SS_lib_type RF --left Scorpion_R1.fastq.gz --right Scorpion_R2.fastq.gz --CPU 6 --max_memory 60G --trimmomatic --full_cleanup --output ./Scorpion_LIBRARY_trinity; Grabherr et al. 2011), removing the adaptors with Trimmomatic v.0.36 (Bolger et al. 2014) and assessing the quality of cleaned raw reads with FastQC v.0.11.5 (Andrews 2010). Protein coding regions within the assembled transcripts were identified using TransDecoder v. 5.3.0 (TransDecoder.LongOrfs -t Scorpion_LIBRARY_trinity.fasta -m 75; TransDecoder.Predict -t Scorpion_LIBRARY_trinity.fasta; Haas et al. 2013). *De novo* phylogenetic orthology resulted prohibitive for a dataset of this size. To overcome this limitation, we leveraged a dataset of 3564 orthologous loci established for 53 chelicerates and outgroups, as described by Ballesteros and Sharma (2019). This dataset was previously established using a phylogenetically-informed criterion for orthology inference and was extensively investigated for sources of systematic bias and signal (Ballesteros and Sharma 2019). The untrimmed alignment of each pre-computed orthogroup was used to produce a hidden Markov profile using *hmmrbuild* (hmmrbuild dataset_loci.fasta loci) from hmmr package v.3.2.1 (Finn et al. 2011). Each proteome/transcriptome of the species of interest was then searched (hmmrsearch loci scorpion_transcriptomes.fasta > new_scorpion_loci.out) for matches against the collection of profiles with an expectation threshold of $e < 10^{-20}$; for cases with more than one hits per locus, the sequence with the best score was selected, and the corresponding sequence appended to the locus FASTA file aggregating the putative orthologous found in each species.

These putative orthogroups was further refined by comparing each of its sequences against the proteome of the fruit fly *Drosophila melanogaster* (NCBI UP000000803), identifying the most common best hit fruit fly gene and removing from the orthogroup all sequences pointing to a different best-hit with *D. melanogaster*. Note that this filter does not require that *D. melanogaster* is included in an orthogroup.

Phylogenetic methods

From this collection of orthologs, gene trees were estimated using IQTREE v.1.6. (Nguyen et al. 2014) implementing the best-fitting amino acid substitution model inferred by ModelFinderPlus (Kalyaanamoorthy et al. 2017) and 1000 ultrafast bootstrapping replicates (Hoang et al. 2018) (iqtree -s ScorpOrthogroup -m MFP -bb 1000). Subsequently, these orthologs were subject to a relaxed occupancy filtering and finally, each gene tree was visually examined for paralogy, in tandem with validation of homology of ambiguous sequences using SMART-BLAST; when detected, individual paralogs were removed. As an example, the sequence of *M. martensii* (shown in red in Figure A1, below) could be either a paralog or a fragmentary sequence (or both). Upon examination, the sequence turned out to be significantly shorter than the rest of the sequences in the alignment, significantly misaligned, and SMART-BLAST recovered a different annotation for this sequence than for the remaining scorpion sequences. Therefore, it was removed from the alignment.

Because most sequences of *M. martensii* featured this issue (long patristic distances in gene trees, together with fragmentary transcripts and anomalous placement with outgroups), this species was removed from our main analyses and its placement was assessed separately, after retaining a very small number of correctly aligned sequences from this dataset (see below).

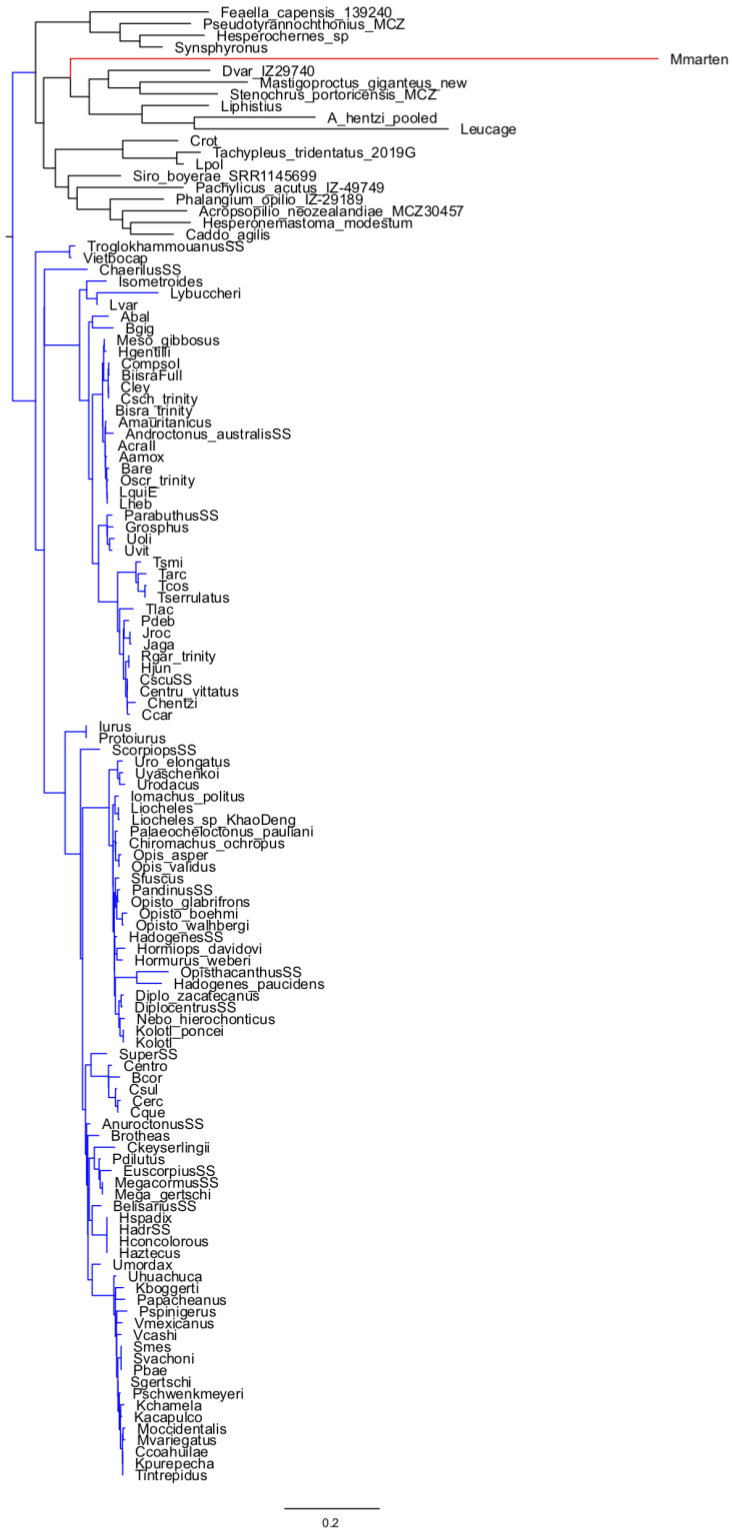

Fig. A1. Exemplar gene tree showing approach to detection of paralogs. Blue: scorpions. Red: Ambiguous sequence of *Mesobuthus martensii* (a highly incomplete Roche 454 pyrosequenced genome).

Three matrices were assembled with a minimal taxon occupancy threshold. For Matrix 1, we retained loci representing at least 115 species per ortholog; for Matrix 2, at least 109 species per ortholog; and for Matrix 3, at least 103 species per ortholog. Matrix 1 consisted of 192 loci and 53,333 sites (>95% complete), Matrix 2 consisted of 424 loci and 114,188 sites (>90% complete), and Matrix 3 consisted of 660 loci and 185,631 sites (>85% complete). Phylogenetic inference of these concatenated matrices was computed with IQ-TREE v.2.0.6 (Minh et al. 2020a) implementing the best-fitting amino acid substitution per partition as selected in our gene tree estimation (-spp). Nodal support was estimated using ultrafast bootstrapping (Hoang et al. 2018), and concordance factors (Minh et al. 2020b). Using the recollection of gene trees, we calculated the gene concordance factor (gCF) and the site concordance factor (sCF) using 100 quartets (e.g. iqtree2 -t AL115.concat.treefile.tree --gcf AL115.loci.treefile.trees -s ScorpAL115.phy --scf 100 --prefix concord_AL115 -T 4). Species tree estimation of the constituent orthologs of the three matrices were generated using the collection of ML gene trees and computed with ASTRAL v.3 (e.g. java -jar astral.5.5.7.jar -i all ready_AL115.tre -o Astral_AL115.tre; Mirarab and Warnow 2015). Lastly, while Bayesian inference analysis was explored for Matrix 3 (>95 complete) using PhyloBayes-mpi v.1.7 (Lartillot et al. 2013) under a CAT + GTR + Γ_4 model (mpirun -np 4 pb_mpi -d AL103.phy -cat -gtr -dgam 4 -dc -t start.tre chtc_scorpio_run) failed to converge after over eight months of computation time on four independent chains; results from the PhyloBayes-mpi run are not shown.

To explore information content and identify potential biases in our phylogenomic matrices, we analyzed our three main datasets using Phykit v.1.5.0 (Steenwyk et al. 2021). Metrics compared across loci in the three matrices consisted of the number of sites per locus, the number of sites without gaps (for i in *.fa; do phykit aln_len_no_gaps $i > Alignment_length/${i%%.*}_aln_len.txt; done), the number of parsimony-informative sites per locus (for i in *.fa; do phykit pis $i > ps-sites/${i%%.*}_ps.txt; done), bipartition support per locus (for i in *.tre; do phykit bss $i > Bipartition/${i%%.*}_bp.txt; done), and long branch score per locus (for i in *.tre; do phykit lb_score $i -verbose > LB_scores/${i%%.*}_lb_ext.txt; done) (Fig. S1). To compare saturation curves (Figs. S2, S3), we constructed plots of uncorrected versus model-correct patristic distances of individual genes. For these plots, we calculated the slope and the correlation of the regression (R^2) using TreSpEx v.1.1 (perl TreSpEx.v1.pl -fun g -ipt AL115trees.txt -ipa AL115alignments.txt -path ./; Struck, 2014), as well as a script previously published by our team (Ballesteros et al. 2019).

Phylogenetic analyses for data-poor terminals

To further explore the validity of higher level buthid systematics, previously defined on the basis of trichobothrial position on the surface of the pedipalps (*sensu* Fet et al. 2005), we searched GenBank for molecular data available for phylogenetically significant scorpion genera and species not sequenced in this study (Supplementary Table S4). We add nine RNA-Seq datasets and one

Sanger-sequenced EST dataset. The orthology inference of the 10 species was conducted as for the main analyses, using the collection of orthologs of our Matrix 2. This augmented matrix is henceforth referred to as “M2plus”.

In addition, we thereafter added Sanger-sequenced data for 10 species (representing buthid genera for which RNA-seq datasets are not available). Sanger-sequenced loci included in our analyses were cytochrome *c* oxidase subunit I (COI), 16S ribosomal RNA, and 18S rRNA. Sequences of these loci were also included for the rest of our study taxa, where available. The resulting matrix (“M2.plus.sanger”) was analyzed using maximum likelihood.

Preliminary phylogenetic analyses of the M2plus and M2.plus.sanger matrices were performed using IQ-TREE, implementing the best-fitting nucleotide substitution model inferred with ModelFinderPlus, and ultrafast bootstrapping (iqtree -spp AlignmentM2p.sanger.nex -bb 1000).

Divergence time estimation

It is well known that performing divergence time estimation with large, modern datasets is notoriously computationally intensive. Thus, Matrix 1 was selected to estimate dates of divergence based on its high taxon occupancy and lower values of missing data. Divergence time estimation was performed using mcmctree v.4.8 (mcmctree mcmctree_AL103.ctl) and codeml v.4.8 (codeml tmp0001.ctl) from the PAML software package v.4.8 (Yang 2007) using the approximate likelihood method (dos Reis and Yang 2011, 2019). The input tree was the best ML topology from the analysis of Matrix 2 (selected for its resolution of buthid internal relationships) and was time-calibrated using 15 calibration points. These points were selected based on several references and are listed in the Supplementary Table S5. Nine outgroup calibration points were implemented as minimum bounds with uniform priors; six scorpion calibration points were implemented as with minimum and maximum bounds; and the root age was implemented as a hard maximum bound. A conservative age constraint on the basal diversification of Arachnida was applied (see *Fossil calibrations*, below).

As suggested by other studies (i.e. Kawahara et al. 2019), the Dirichlet-Gamma density (dos Reis et al. 2014) was used to set the prior on the molecular rate with the default parameters ($\alpha_\mu = 2$, $\beta_\mu = 6$, $\alpha = 1$). Similarly, the default parameters for the birth-death process were kept ($\lambda = 1$, $p = 0.1$). Independent-rates and the correlated rates models were selected to perform the divergence time estimation. Hessian matrices were calculated with codeml using empirical base frequencies and the LG substitution model with 5 rate categories. A burn-in of 25,000, sample frequency of 100, and a sample size of 25,000 (resulting in a 2.5 million generations) for each of the two clock models was implemented. Each analysis was repeated four times, with the convergence subsequently evaluated in Tracer v. 1.7.1 (Rambaut et al. 2018) and by plotting the node ages against each other in R (data available upon request). Lastly, the four chains were merged to achieve large effective sample sizes (ESS > 200) and produce the summary tree. The resulting topology was plotted using the function *MCMC.tree.plot* from the R package MCMCtreeR v.1.1 (Puttick 2019).

Fossil calibrations

The oldest putative fossil scorpion, *Parioscorpio venator*, was recently discovered and dates to the Silurian (436.5-437.5 Mya; Wendruff et al. 2020), slightly pushing back the age of the oldest stem-group Scorpiones as inferred from fossils like *Dolichophonus loudenensis* and *Eramoscorpius brucensis*. However, recently Anderson et al. (2021) showed evidence suggesting *P. venator* is not a scorpion. Therefore, for our analysis, we used the date of *E. brucensis* to set the minimum age for the stem-group. The oldest crown group scorpion (Orthosterni) is Carboniferous in age (*Protoischnurus axelrodorum*) (reviewed by Wolfe et al. 2016). We constrained the stem age of scorpions (divergence from outgroup taxa) using a soft minimum of 435.15 Mya and a soft maximum of 514 Mya, with the upper bound following an established calibration strategy for arthropods (Wolfe et al. 2016). We constrained crown Orthosterni with a soft maximum age of 313.7 Mya and a soft minimum age of 112.6 Mya, based on the age of *Compsoscorpius buthiformis*, a fossil Scorpionoidea (Poiton et al. 2012). Given the clear affinity of *Protoischnurus axelrodorum* as a lineage within Iurida (Menton 2007), Iurida was also constrained using soft bounds of 112.6 to 313.7 Mya. Chaerilidae was constrained using a soft minimum age of 98.17 Mya, based on the age of *Electrochaerilus buckleyi* (Santiago-Blay et al. 2004a) and a soft maximum age of 313.7 Mya. We constrained Buthoidea using a soft minimum of 49.26 Mya, based on the age of *Uintascorpio halandrasi* (Perry 1995, Santiago-Blay et al. 2004b) and a soft maximum age of 313.7 Mya, given the sister group relationship of Buthida and Iurida. Finally, the superfamily

Scorpionoidea was constrained with a soft minimum of 112.6 Mya, based on the age of *Compsoscorpius buthiformis*, and a soft maximum of 313.7 Mya. Further discussion of these fossils is provided in a recent review (Howard et al. 2019). Ten additional outgroup calibrations were deployed for the remaining chelicerate orders, using only soft minimum calibrations. We constrained the crown group of Opiliones using the soft minimum age of 411 Mya, based on the harvestman fossil *Eophalangium sheari* (Garwood et al. 2014), the divergence of Eupnoi harvestmen with a soft minimum age of 305 Mya, based on the age of *Macrogyion cronus* (Garwood et al. 2011); and the divergence of Dyspnoi harvestmen with a soft minimum age of 305 Mya, based on the age of *Ameticos scolos* (Garwood et al. 2011). The age of Araneae was calibrated with a soft minimum age of 386 Mya, based on the fossil *Attercopus fimbriunguis* (Selden et al. 2008, Huang et al. 2018). The stem-group age of Mesothelae was calibrated with a soft minimum age of 305 Mya, based on the unambigious mesothele fossil *Palaeothele montceauensis* (Selden 1996). The stem-group age of Amblypygi was bounded with a soft minimum age of 312 Mya based on the fossils *Graeophonus anglicus* and *G. carbonarius* (Dunlop et al. 2007). The crown group of Pseudoscorpiones was calibrated with a soft mimimum age of 392 Mya, based on the age of *Dracochela deprehendor* (Schawaller et al. 1991). Finally, the stem-group age of Xiphosura was constrained with a soft minimum age of 445 Mya, corresponding to the age of *Lunataspis aurora* (Rudkin et al. 2008).

Maximum bounds were omitted for outgroup orders, because these are nuisance parameters and the the fossil record of many of these groups is too poor to facilitate the selection of reasonable maximum bounds. As an intuitive example, the oldest known arachnid fossils are those of scorpions from the Silurian (e.g., *Eramoscorpius brucensis*, ca. 435 Mya). It has been recently shown that scorpions are likely nested deeply within Arachnopulmonata, as the sister group of pseudoscorpions (Ontano et al. 2021). It then stands to reason that (at least stem-group) Pseudoscorpiones and Tetrapulmonata had diversified by the Silurian as well. The absence of groups like Pedipalpi for another ca. 120 million years after the appearance of *E. brucensis* implies that the fossil record of terrestrial chelicerates is too sparse for reasonable application of maximum age bounds. Given that the diversity of these outgroup orders is also poorly sampled, we restricted the use of maximum age bounds only to scorpions, which have a comparatively richer Paleozoic record.

Gene tree analyses and molecular evolution of venom scorpion peptides

Cysteine-stabilized α-helix and β-sheet fold (CSαβ), disulfide-directed beta-hairpin (DDH) and inhibitor cystine knot (ICK) homologs from scorpion venom were retrieved from our concatenated transcriptome libraries using a query files with known CSαβ - ICK - DDH sequences from the venom of scorpions (i.e. sodium channel toxins, potassium channel toxins, chloride channel toxins, scorpines, Kunitz-type inhibitors, and calcins). Matching sequences with low e-values ($e < 1 \times 10^{-15}$) were selected. Subsequently, these selected sequences were concatenated with 789 sequences from scorpion venom peptides retrieved from UniProt and InterPro (Supplementary Table S6).

Preliminary ML phylogenetic analyses were conducted using the entire dataset and IQ-TREE (iqtree -s ICK_CSab_DDH_dataset.fasta -m MFP -bb 1000), with the resulting trees analyzed in search of orthologs. We removed sequences retrieved from our transcriptomes that were recovered outside clades with at least one known venom sequence. Our final dataset consisted of 1,353 CS$\alpha\beta$ -ICK scorpion sequences and 41 DDH scorpion toxin sequences as outgroup. Clades were delimitated manually based on the presence of well-known scorpion toxins (Supplementary Table S6). Thus, the sodium channel toxins (NaTx) dataset consisted of 661 sequences, the potassium channel toxins (KTx) dataset of 550, the chloride channel toxins (ClTx) dataset of 56, and the calcin dataset of 74 sequences. Multiple sequence alignments for sequences from each clade were constructed using MAFFT v.7.4 with default parameters (Katoh and Standley 2013) and gene trees were generated using IQ-TREE implementing ModelFinderPlus and ultrafast bootstrapping (e.g. iqtree -s NaTx_dataset.fasta -m MFP -bb 1000). The topology of NaTx (Figure 3B) was plotted and annotated with the Iroki webapp (https://www.iroki.net/; Moore et al. 2020). Our annotations included the names of the parvorders (e.g., Iurida), family (e.g., Pseudochactidae) or buthid species groups. In addition, we included the names of the NaTx clades recovered from our ML analyses. Lastly, we include the annotations for sequences with known functions and affinities.

The signal peptides, propeptides and mature peptides were predicted for the sequences in each clade using SpiderP from Arachnoserver (Herzig et al 2010). To determine if convergent sites predates the origin of different clades of mammal-active toxins within NaTx, motifs from the mature peptide (the active component of the toxin) were generated using the Multiple Em for Motif Elicitation server (MEME v.5.1.1 at http://meme-suite.org/tools/meme; Bailey et al. 2015). Gene trees and multiple sequence alignment were plotted using the extended R package ggmsa v.1.0.2 from ggplot2 v.3.3.5 (Wickham, 2016) with the function *geom_facet*. Consensus sequences were obtained for each subclade recovered in our gene tree analyses using JalView v.2.11 (Waterhouse et al. 2009). These consensus sequences were then aligned to one representative sequence with known affinity from each clade in JalView (Supplementary Figure S19).

Additionally, the mature peptides of the amino acid sequences from the two main clades recovered in the ML analysis of the NaTx (Aah2-like and Cn2-like) were used for CLANS v.29.05.2012 cluster analysis (java -jar clans,jar clans.conf; Frickey and Lupas 2004) with the default parameters as stated in the configuration file.

The distribution of the different scorpion toxins in their corresponding clades (as recovered by our gene tree analyses), and the species hierarchical taxonomic category were mapped as an alluvial plot with the R package ggplot2 and the function *geom_alluvium*. In addition, the diversity of selected transcripts (e.g. number of NaTx, calcins, or KTx) was mapped as a function of a heatmap and the scorpion phylogeny with the extended R package ggtree v.2.5.1 (function *gheatmap*; Yu, 2020) from ggplot2.

Phylostratigraphic bracketing approach to infer the origins and ages of mammal-active toxins

To infer the origins of mammal-active toxins in scorpion venom, we used phylostratigraphic bracketing, an approach that uses minimum-spanning clades as a minimum age estimate for age of origin. Based on our annotated NaTx with Iroki, we traced the origin of toxins present in the venom of closely related scorpions. As a hypothetical example, if a toxin with known mammalian ion channel affinity belongs to a *Tityus* species (i.e., was sequenced from a *Tityus* and was recovered in a cluster containing other venom sequences of *Tityus* species), we inferred the origin of that toxin to be at least present by the stem-age of that node (the stem-age of *Tityus*). Using this approach, we conservatively identified eight different origins of mammal sodium channel affinity, which corresponded to four nodes in the species tree: *Centruroides*, *Tityus*, *Parabuthus* and the *Buthus* group. We corroborated independent origins of mammal-active toxins using the output of CLANS clustering, which recovered several well-separated clusters of NaTx sequences. When annotated for toxin affinity, mammal-active toxins formed eight independent clusters, reinforcing the inference of independent origins of mammal ion channel affinity.

To infer the age of the mammal-active toxins in scorpion venom, we used the stem age of the most inclusive buthid clades containing those species with known mammal-active toxins as a proxy for the minimum estimate of gene age. The posterior distribution of the stem ages of *Centruroides*, *Tityus*, *Parabuthus* and the *Buthus* group were retrieved from our mcmctree results, and plotted using MCMCtreeR.

To compare these results to the ages of scorpion predators, we obtained the 95% Highest Posterior Density (95% HPD) interval for the node ages of Didelphimorphia, Eulipotyphia, Chiroptera, Carnivora and Rodentia from the phylogenetic works of Meredith et al. (2011) and Upham et al. (2019). These HPD intervals were plotted using MCMCtreeR to evaluate overlap and temporal sequence of toxin and predator origins.

Supplementary References

Anderson, E.P., Schiffbauer, J.D., Jacquet, S.M., Lamsdell, J.C., Kluessendorf, J., Mikulic, D.G. 2021. Stranger than a scorpion: A reassessment of *Parioscorpio venator*, a problematic arthropod from the Llandoverian Waukesha Lagerstätte. Palaeontology 64: 429-474.

Andrews S. 2010. FastQC: a quality control tool for high throughput sequence data.

Bailey T.L., Johnson J., Grant C.E., Noble W.S. 2015. The MEME Suite. Nucleic Acids Res. 43(W1):W39–W49.

Ballesteros J.A., Sharma P.P. 2019. A Critical Appraisal of the Placement of Xiphosura (Chelicerata) with Account of Known Sources of Phylogenetic Error. Syst. Biol. 33:440–22.

Ballesteros, J.A., Santibáñez-López, C.E., Kovác, L., Gavish-Regev, E., Sharma, P.P. 2019. Ordered phylogenomic subsampling enables diagnosis of systematic errors in the placement of the enigmatic arachnid order Palpigradi. Proc. R. Soc. B 286: 20192426.

Biasini M., Bienert S., Waterhouse A., Arnold K., Studer G., Schmidt T., Kiefer F., Cassarino T.G., Bertoni M., Bordoli L., Schwede T. 2014. SWISS-MODEL: modelling protein tertiary and quaternary structure using evolutionary information. Nucleic Acids Res. 42(W1): W252-258.

Bolger A.M., Lohse M., Usadel B. 2014. Trimmomatic: a flexible trimmer for Illumina sequence data. Bioinformatics. 30:2114–2120.

dos Reis M.D., Yang Z. 2011. Approximate Likelihood Calculation on a Phylogeny for Bayesian Estimation of Divergence Times. Mol. Biol. Evol. 28:2161–2172.

dos Reis M., Yang Z. 2019. Bayesian Molecular Clock Dating Using Genome-Scale Datasets. In: Anisimova M. (eds) Evolutionary Genomics. Methods in Molecular Biology, vol 1910. Humana, New York, NY. Pp 309-330.

dos Reis M., Zhu T., Yang Z. 2014. The Impact of the Rate Prior on Bayesian Estimation of Divergence Times with Multiple Loci. Syst. Biol. 63:555–565.

Dunlop J.A., Zhou G.R.S., Braddy S.J. 2007. The affinities of the Carboniferous whip spider *Graeophonus anglicus* Pocock, 1911 (Arachnida: Amblypygi). Earth Environ. Sci. Trans. R. Soc. Edinb. 98:165–178.

Fet V., Soleglad M.E., Lowe G. 2005. A new trichobotrhial character for the high-level systematics of Buthoidea (Scorpiones: Buthida). Euscorpius. 23:1–40.

Finn R.D., Clements J., Eddy S.R. 2011. HMMER web server: interactive sequence similarity searching. Nucleic Acids Res. 39:W29–W37.

Frickey T., Lupas A. 2004. CLANS: a Java application for visualizing protein families based on pairwise similarity. Bioinformatics 20(18):3702–3704.

Garwood R.J., Sharma P.P., Dunlop J.A., Giribet G. 2014. A Paleozoic stem group to mite harvestmen revealed through integration of phylogenetics and development. Curr. Biol. 24:1017–1023.

Garwood R.J, Dunlop J.A., Giribet G., Sutton M.D. 2011. Anatomically modern Carboniferous harvestmen demonstrate early cladogenesis and stasis in Opiliones. Nat. Commun. 2:444.

Grabherr M.G., Haas B.J., Yassour M., Levin J.Z., Thompson D.A., Amit I., Adiconis X., Fan L., Raychowdhury R., Zeng Q., Chen Z., Mauceli E., Hacohen N., Gnirke A., Rhind N., di Palma F., Birren B.W., Nusbaum C., Lindblad-Toh K., Friedman N., Regev A. 2011. Full-length transcriptome assembly from RNA-Seq data without a reference genome. Nat. Biotechnol. 29:644–652.

Haas B.J., Papanicolaou A., Yassour M., Grabherr M., Blood P.D., Bowden J., Couger M.B., Eccles D., Li B., Lieber M., MacManes M.D., Ott M., Orvis J., Pochet N., Strozzi F., Weeks N., Westerman R., William T., Dewey C.N., Henschel R., LeDuc R.D., Friedman N., Regev A. 2013. De novo transcript sequence reconstruction from RNA-seq using the Trinity platform for reference generation and analysis. Nat. Protocols. 8:1494–1512.

Herzig V., Wood D.L.A., Newell F., Chaumeil P.A., Kaas Q., Binford G.J., Nicholson G.M., Gorse D., King G.F. 2010. ArachnoServer 2.0, an updated online resource for spider toxin sequences and structures. Nucleic Acids Res. 39:D653–D657.

Hoang, D.T., Chernomor, O., von Haeseler, A., Minh, B.Q., Vinh, L.S. 2018. UFBoot2: Improving the ultrafast bootstrap approximation. Mol. Biol. Evol. 35:518–522.

Howard R.J., Edgecombe G.D., Legg D.A., Pisani D., Lozano-Fernandez J. 2019. Exploring the evolution and terrestrialization of scorpions (Arachnida: Scorpiones) with rocks and clocks. Org. Div. Evol. 19:71–86.

Huang D., Hormiga G., Cai C., Su Y., Yin Z., Xia F., Giribet G. 2018. Origin of spiders and their spinning organs illuminated by mid-Cretaceous amber fossils. Nature Ecol. Evol. 2:623–627.

Kalyaanamoorthy S., Minh B.Q., Wong T.K.F., Haeseler von A., Jermiin L.S. 2017. ModelFinder: fast model selection for accurate phylogenetic estimates. Nat. Methods. 14:587–589.

Kawahara A.Y., Plotkin D., Espeland M., Meusemann K., Toussaint E.F.A., Donath A., Gimnich F., Frandsen P.B., Zwick A., Reis dos M., Barber J.R., Peters R.S., Liu S., Zhou X., Mayer C., Podsiadlowski L., Storer C., Yack J.E., Misof B., Breinholt J.W. 2019. Phylogenomics reveals the evolutionary timing and pattern of butterflies and moths. Proc. Natl. Acad. Sci. U.S.A. 116:22657–22663.

Katoh, K., Standley, D.M. 2013. MAFFT Multiple Sequence Alignment Software version 7: Improvements in Performance and Usability. Mol. Biol. Evol. 30: 772-780.

Lartillot N., Rodrigue N., Stubbs D., Richer J. 2013. PhyloBayes MPI: Phylogenetic Reconstruction with Infinite Mixtures of Profiles in a Parallel Environment. Syst. Biol. 62:611–615.

Menon F. 2007. Higher systematics of scorpions from the Crato Formation, Lower Cretaceous of Brazil. Palaeontology 50:185–195.

Meredith, R.W., Janecka, J.E., Gatesy, J., Ryder, O.A., Fisher, C.A., Teeling, E.C., Goodbla, A., Eizirik, E., Simão, T.L., Stadler, T. & Rabosky, D.L. 2011. Impacts of the Cretaceous Terrestrial Revolution and KPg extinction on mammal diversification. Science 334(6055): 521-524.

Minh, B.Q., Schmidt, H.A., Chernomor, O., Schrempf, D., Woodhams, M.D., von Haeseler, A., Lanfear, R. 2020a. IQ-TREE 2: New models and efficient methods for phylogenetic inference in the genomic era. Mol. Biol. Evol. 27: 1530-1534.

Minh, B.Q., Hahn, M.W., Lanfear, R. 2020b. New methods to calculate concordance factors for phylonogemic datasets. Mol. Biol. Evol. 37: 2727-2733.

Mirarab S., Warnow T. 2015. ASTRAL-II: coalescent-based species tree estimation with many hundreds of taxa and thousands of genes. Bioinformatics. 31:44–52.

Moore R.M., Harrison A.O., McAllister S.M., Polson S.W., Wommack K.E. 2020. Iroki: automatic customization and visualization of phylogenetic trees. PeerJ 8:e8584.

Nguyen L.-T., Schmidt H.A., Haeseler von A., Minh B.Q. 2014. IQ-TREE: A Fast and Effective Stochastic Algorithm for Estimating Maximum-Likelihood Phylogenies. Mol. Biol. Evol. 32:268–274.

Ontano, A.Z., Gainett, G., Aharon, S., Ballesteros, J.A., Benavides, L.R., Corbett, K.F., Gavish-Regev, E., Harvey, M.S., Monsma, S., Santibáñez-López, C.E., Setton, E.V., Zehms, J.T., Zeh, J.A., Zeh, D.W., Sharma P.P. 2021. Taxonomic sampling and rare genomic changes overcome long-branch attraction in the phylogenetic placement of pseudoscorpions. Mol. Biol. Evol. 38: 2446-2467.

Perry M.L. 1995. Preliminary description of a new fossil scorpion from the Middle Eocene Green River Formation, Rio Blanco County, Colorado. In: Dayvault RD, Averett WR (eds.), *The Green River Formation in Piceance Creek and Eastern Uinta Basins Field Trip* (pp. 131–133). Grand Junction: Grand Junction Geological Society.

Pointon M.A., Chew D.M., Ovtcharova M., Sevastopulo G.D., Crowley Q.G. 2012. New high-precision U–Pb dates from western European Carboniferous tuffs; implications for time scale calibration, the periodicity of late Carboniferous cycles and stratigraphical correlation. J. Geol. Soc. Lond. 169:713–721.

Puttick M.N. 2019. MCMCtreeR: functions to prepare MCMCtree analyses and visualize posterior ages on trees. Bioinformatics. 35:5321–5322.

Rambaut A., Drummond A.J., Xie D., Baele G., Suchard M.A. 2018. Posterior Summarization in Bayesian Phylogenetics Using Tracer 1.7. Syst. Biol. 67:901–904.

Rudkin D.M., Young G.A., Nowlan G.S. 2008. The oldest horseshoe crab: a new xiphosurid from late Ordovician Konservat-Lagerstätten deposits, Manitoba, Canada. Palaeontology 51:1–9.

Santiago-Blay J.A., Fet V., Soleglad M.E., Anderson S.R. 2004a. A new genus and subfamily of scorpions from Cretaceous Burmese amber (Scorpiones: Chaerilidae). Rev. Ibér. Aracnol. 9:3–14.

Santiago-Blay J.A., Soleglad M.E., Fet V. 2004b. A redescription and family placement of *Uintascorpio* Perry, 1995 from the Parachute Creek Member of the Green River Formation (Middle Eocene) of Colorado, USA (Scorpiones: Buthidae). Rev. Ibér. Aracnol. 10:7–16.

Santibáñez-López C., Ontano A., Harvey M., Sharma P. 2018a. Transcriptomic Analysis of Pseudoscorpion Venom Reveals a Unique Cocktail Dominated by Enzymes and Protease Inhibitors. Toxins. 10:207–12.

Santibáñez-López C.E., González-Santillán E., Monod L., Sharma P.P. 2019. Phylogenomics facilitates stable scorpion systematics_ Reassessing the relationships of Vaejovidae and a new higher-level classification of Scorpiones (Arachnida). Mol. Phylogen. Evol. 135:22–30.

Santibáñez-López C.E., Kriebel R., Ballesteros J.A., Rush N., Witter Z., Williams J., Janies D.A., Sharma P.P. 2018b. Integration of phylogenomics and molecular modeling reveals lineage-specific diversification of toxins in scorpions. PeerJ. 6:e5902–23.

Schawaller W., Shear W.A., Bonamo P.M. 1991. The first Paleozoic pseudoscorpions (Arachnida, Pseudoscorpionida). Amer. Mus. Novitates 3009:1–17.

Selden P.A. 1996 First fossil mesothele spider, from the Carboniferous of France. Rev. Suisse Zool. hors. série:585–596.

Selden P.A., Shear W.A., Sutton M.D. 2008. Fossil evidence for the origin of spider spinnerets, and a proposed arachnid order. Proc. Natl. Acad. Sci. USA 105:20781–20785.

Sharma P.P., Fernández R., Esposito L.A., González-Santillán E., Monod L. 2015. Phylogenomic resolution of scorpions reveals multilevel discordance with morphological phylogenetic signal. Proc. Biol. Sci. 282:20142953.

Sharma P.P., Kaluziak S.T., Pérez-Porro A.R., González V.L., Hormiga G., Wheeler W.C., Giribet G. 2014. Phylogenomic interrogation of arachnida reveals systemic conflicts in phylogenetic signal. Mol. Biol. Evol. 31:2963–2984.

Steenwyk, J. L., Buida, T. J., Labella, A. L., Li, Y., Shen, X. X., & Rokas, A. 2021. PhyKIT: a broadly applicable UNIX shell toolkit for processing and analyzing phylogenomic data. Bioinformatics *1*-7.

Struck, T.H. 2014. TreSpEx-detection of misleading signal in phylogenetic reconstructions based on tree information. Evol. Bioinformatics 10: 51-67.

Upham N.S., Esselstyn J.A., Jetz W. 2019. Inferring the mammal tree: Species-level sets of phylogenies for questions in ecology, evolution, and conservation. PLoS Biol. 17:e3000494–44.

Waterhouse, A.M., Procter, J.B., Martin, D.M.A., Clamp, M., Barton, G.J. 2009. Jalview version 2 – a multiple sequence alignment editor and analysis workbench. Bioinformatics 25: 1189-1191.

Wendruff A.J., Babcock L.E., Wirkner C.S., Kluessendorf J., Mikulic D.G. 2020. A Silurian ancestral scorpion with fossilised internal anatomy illustrating a pathway to arachnid terrestrialisation. Sci. Rep. 10:14.

Wickham, H. 2016. ggplot2: Elegant Graphics for Data Analysis. Springer-Verlag New York.

Wolfe J.M., Daley A.C., Legg D.A., Edgecombe G.D. 2016 Fossil calibrations for the arthropod Tree of Life. Earth-Sci. Rev. 160:43–110.

Yang Z. 2007. PAML 4: Phylogenetic Analysis by Maximum Likelihood. Mol. Biol. Evol. 24:1586–1591.

Yu, G. 2020. Using ggtree to visualize data on tree-like structures. Curr. Protocols Bioinformatics 69: e96.

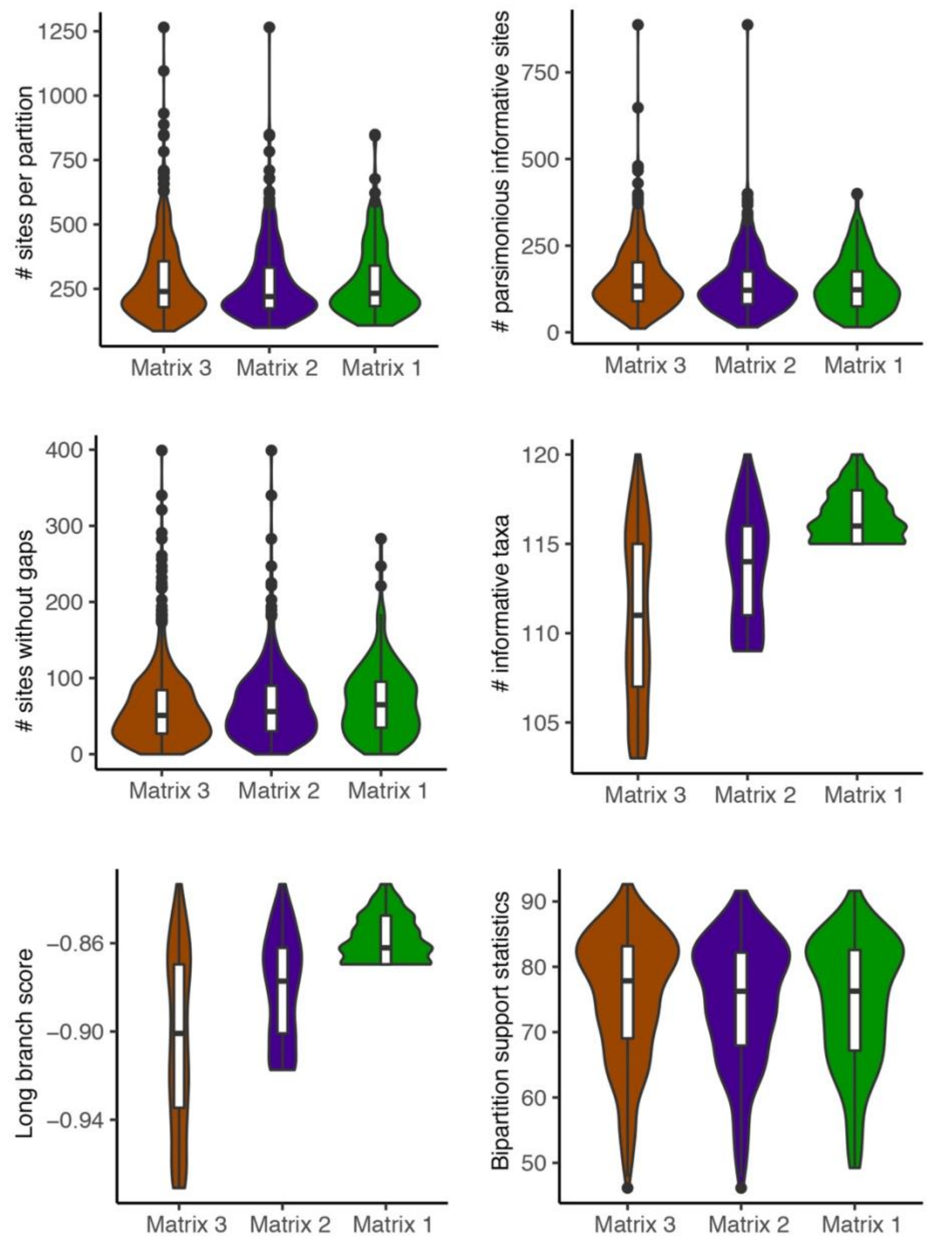

Supplementary Figure S1. Violin plots summarizing information content in the three matrices. The long branch score can be used as a measure of heterogeneity by identifying taxa that can contribute to long branch issues. Similarly, the bipartition support statistics aims to provide certainty among bipartitions within each gene partition.

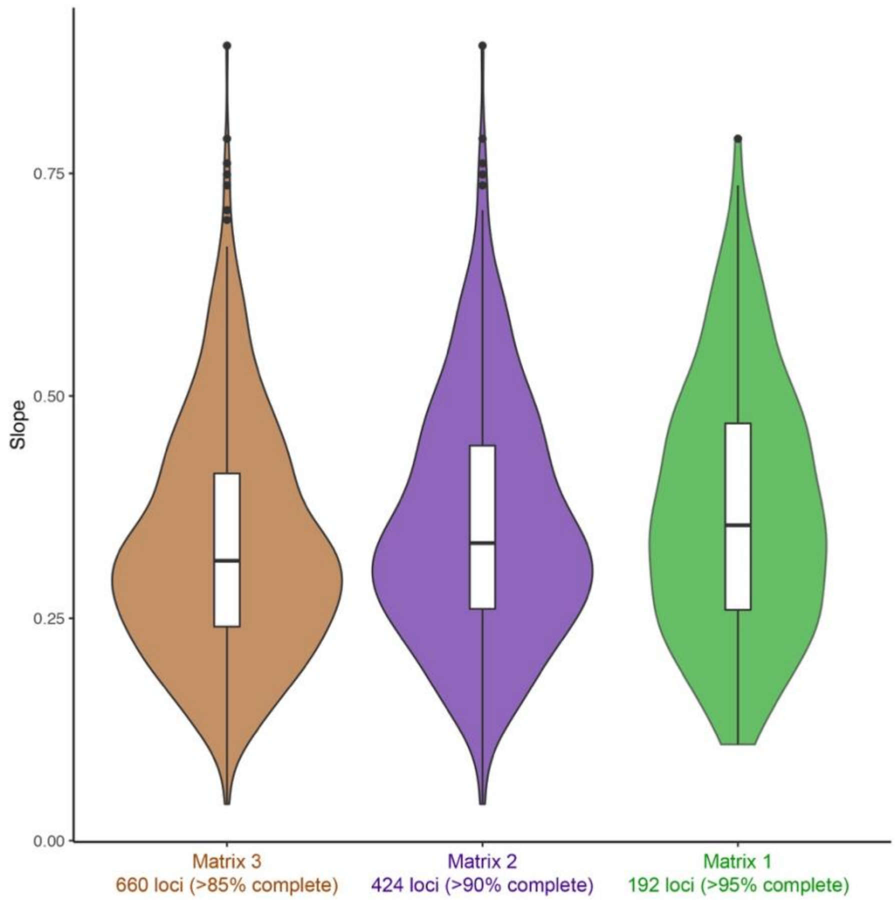

Supplementary Figure S2. Saturation per-locus measured as a function of the slope for genes in Matrices 1-3.

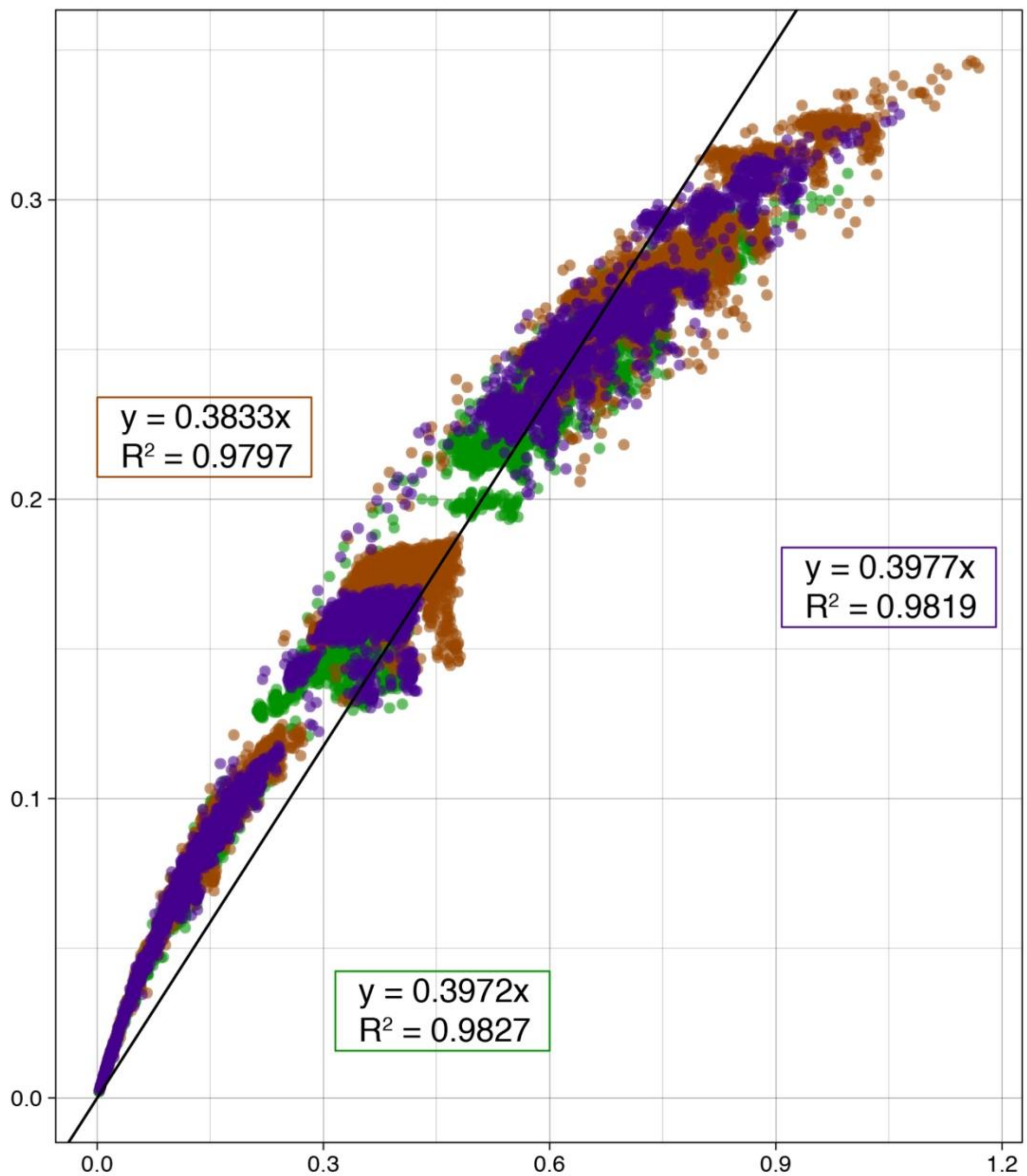

Supplementary Figure S3. Estimations of slope and the correlation coefficient for Matrices 1(green), 2 (purple), and 3 (brown), implementing a y-intercept as shown in Ballesteros et al. (2019).

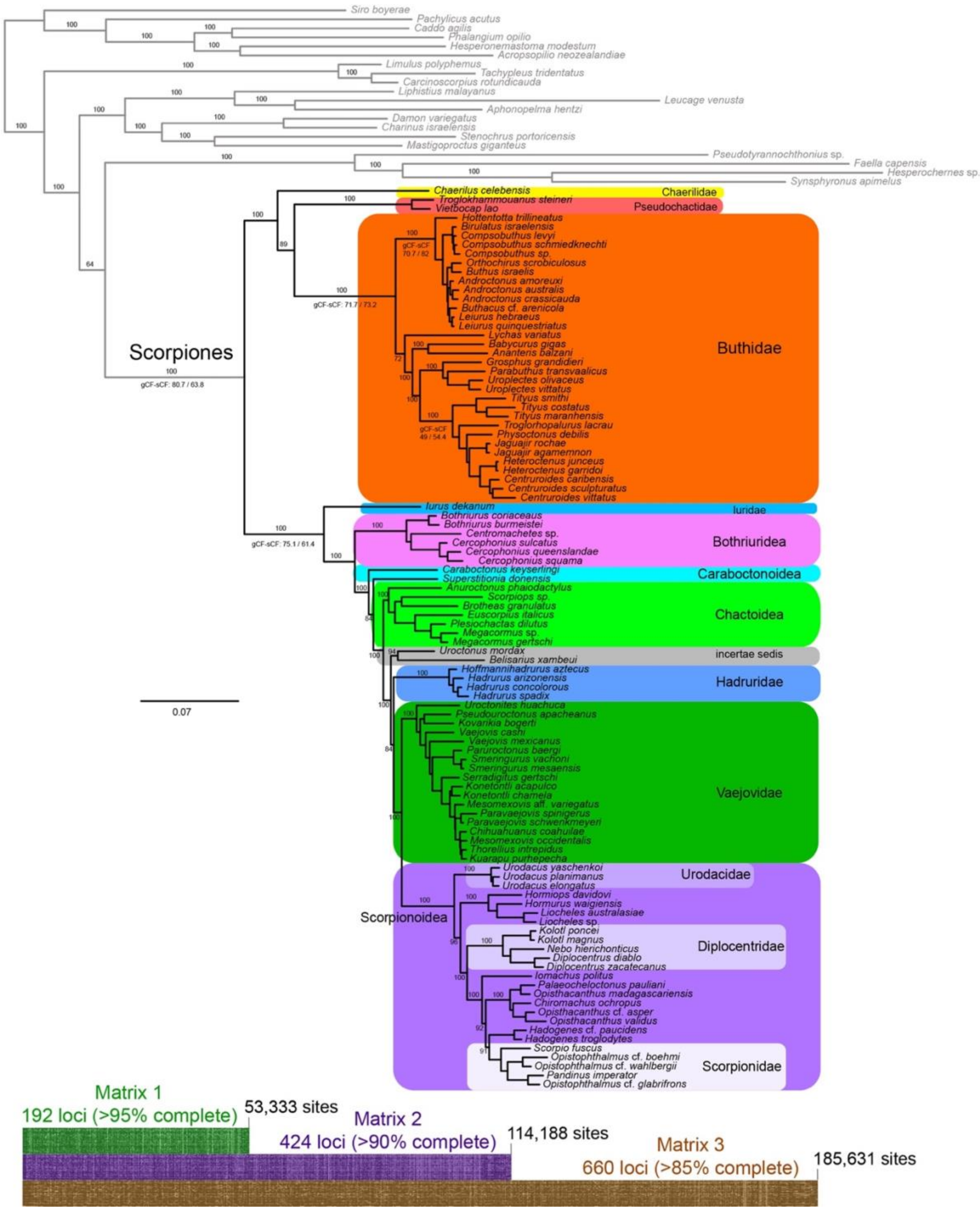

Supplementary Figure S4. Maximum likelihood tree topology recovered from the analysis of 192 loci (Matrix 1). Numbers above nodes indicate bootstrap support values, below nodes indicate gene concordance factor (gCF) and the site concordance factor (sCF). Bottom panel shows an overview of the three matrices.

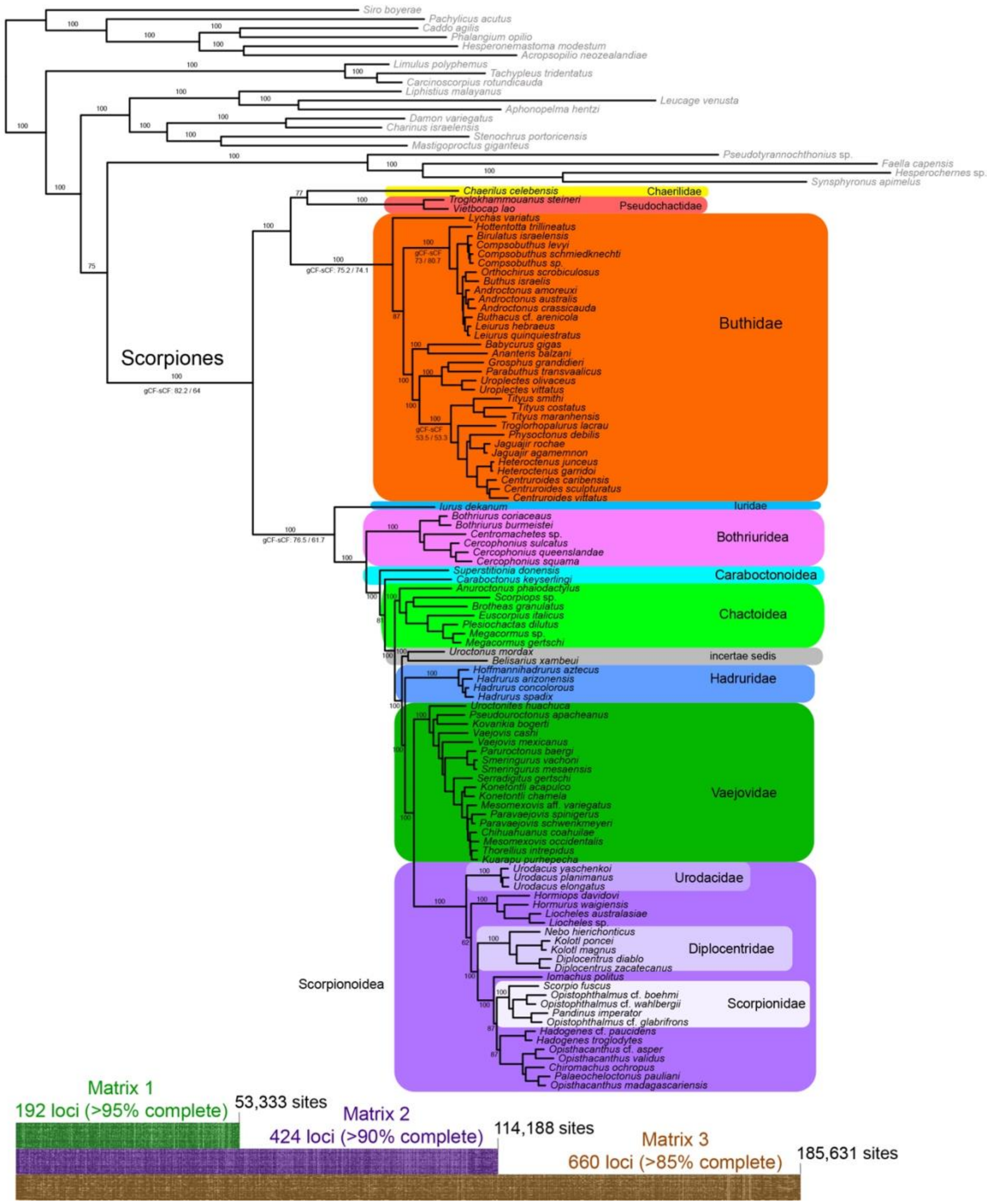

Supplementary Figure S5. Maximum likelihood tree topology recovered from the analysis of 424 loci (Matrix 2). Numbers above nodes indicate bootstrap support values. Bottom panel shows an overview of the three matrices.

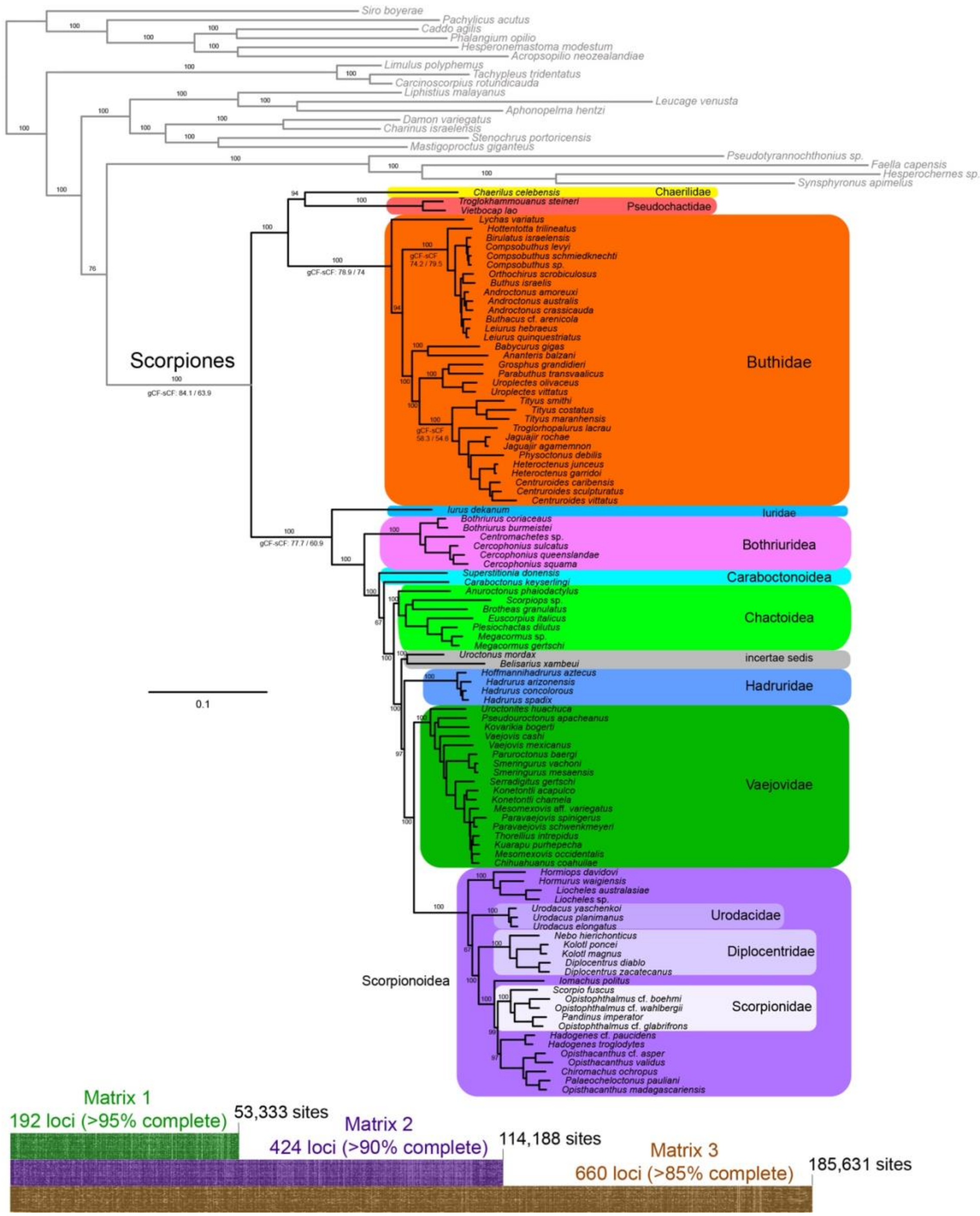

Supplementary Figure S6. Maximum likelihood tree topology recovered from the analysis of 660 loci (Matrix 3). Numbers above nodes indicate bootstrap support values. Bottom panel shows an overview of the three matrices.

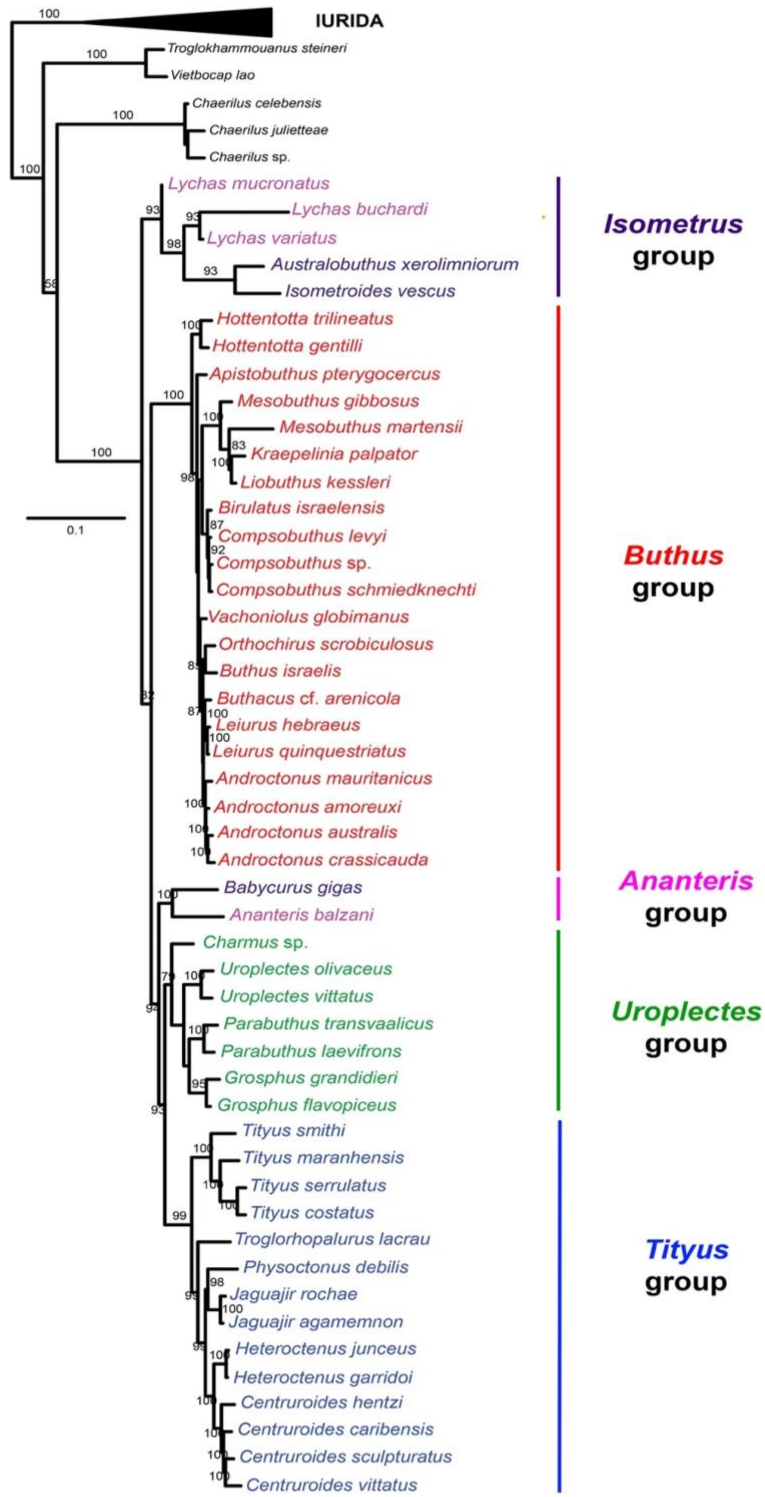

Supplementary Figure S7. Maximum likelihood tree topology of Buthida recovered from the analysis of a combined dataset consisting of 424 genes (Matrix 2) and 2,692 nucleotides corresponding to three genes (18S rRNA, 16S rRNA, and COI). Color coding indicates species groups delimited by Fet et al. (2005).

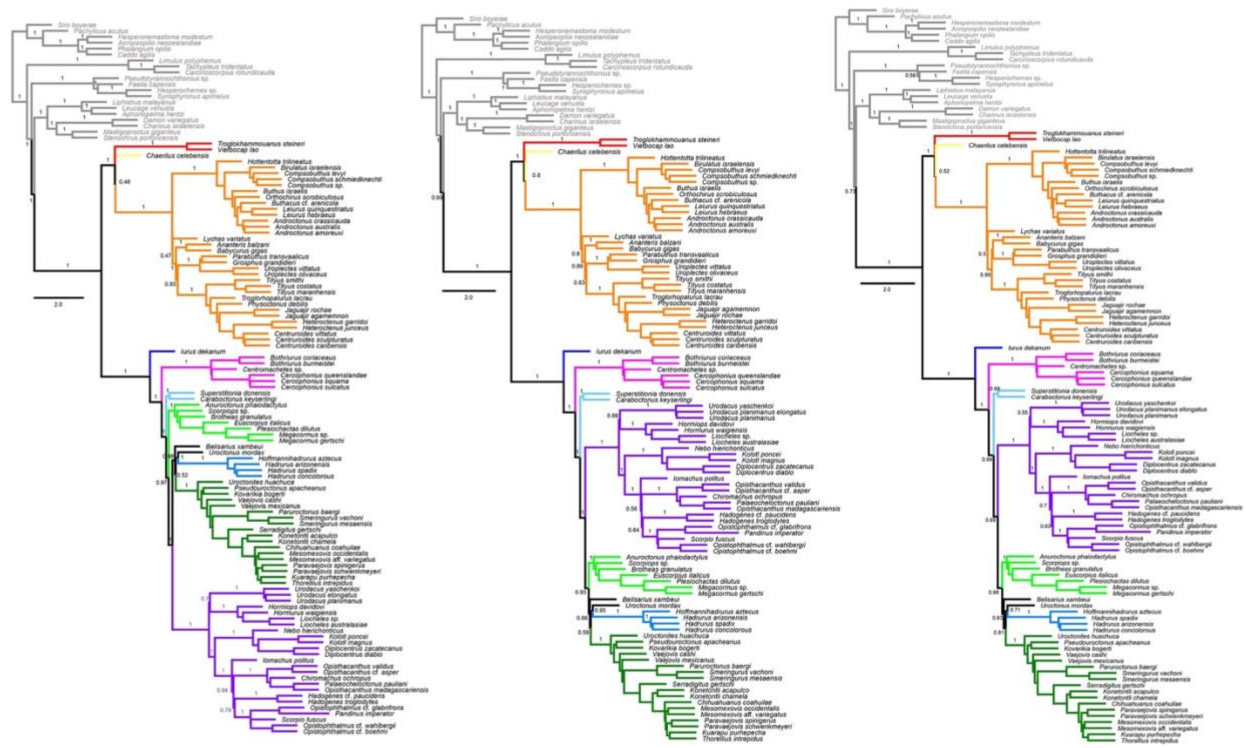

Supplementary Figure S8. ASTRAL trees recovered from gene trees constituting Matrix 1(left), Matrix 2 (center), and Matrix3 (right). Numbers indicate branch support from local posterior probabilities.

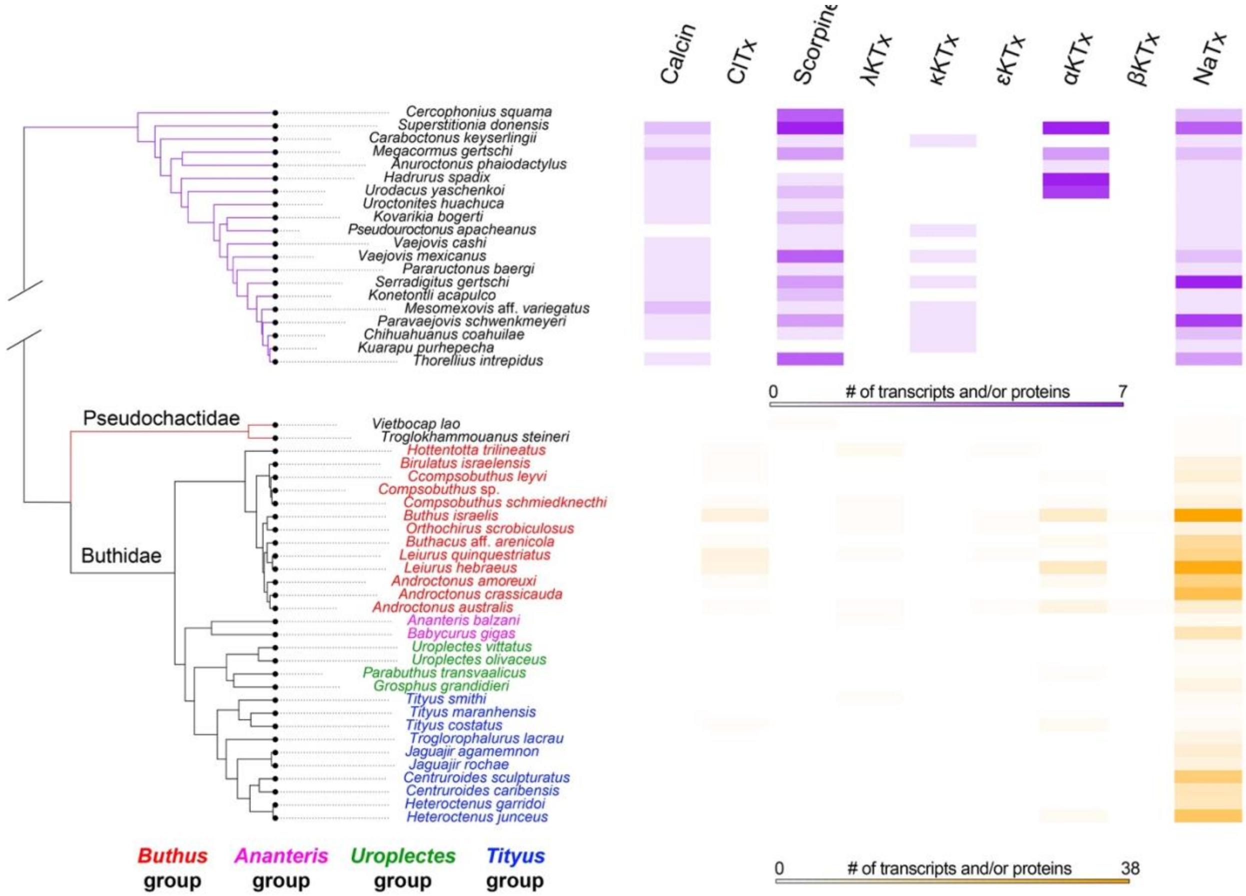

Supplementary Figure S9. Summary of scorpion time tree showing the diversity of venom components in the different families and genera. Data were obtained from transcriptomic resources and databases (UniProt and InterPro).

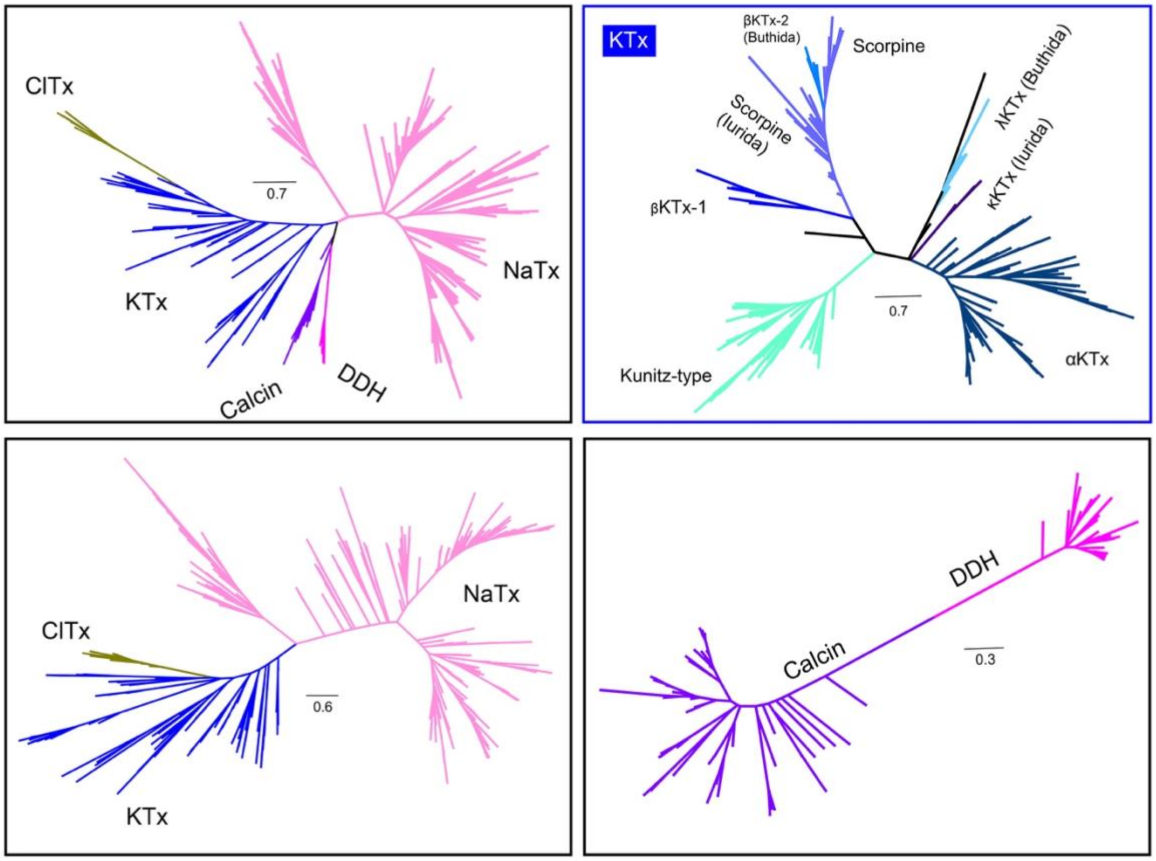

Supplementary Figure S10. Maximum likelihood evolutionary tree for CS$\alpha\beta$-ICK gene families (top left) and KTx gene families (top right). ML evolutionary trees for CS$\alpha\beta$ (bottom left) and ICK-DDH (bottom right) inferred independently from each other.

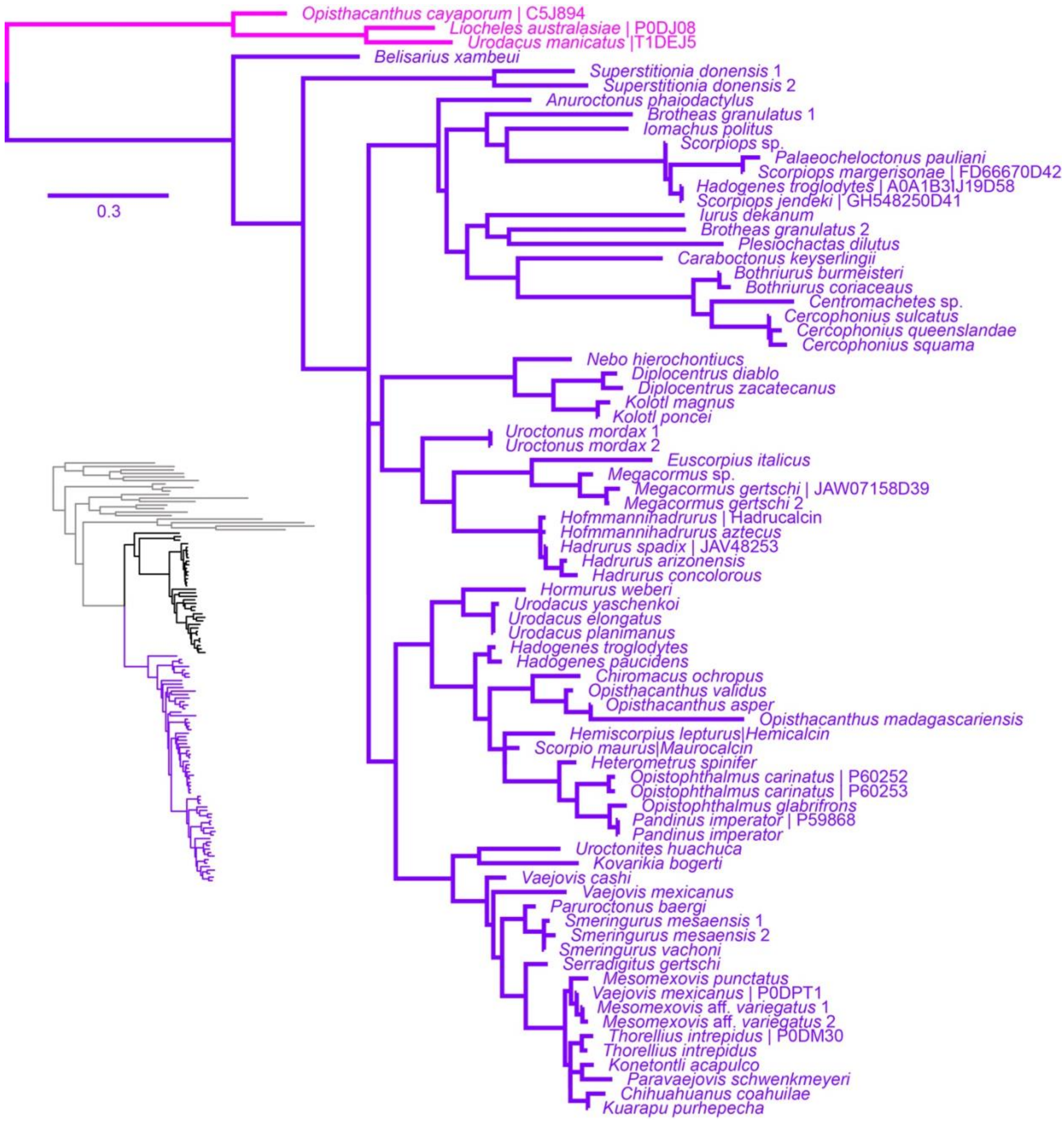

Supplementary Figure S11. Maximum likelihood gene tree recovered from the analysis of 74 ryanodine receptor ligand peptides (calcins) and three disulphide-directed beta-hairpin (DDH) genes as outgroups. Calcins are ubiquitous in iurid scorpion venom as shown on the inset scorpion phylogeny.

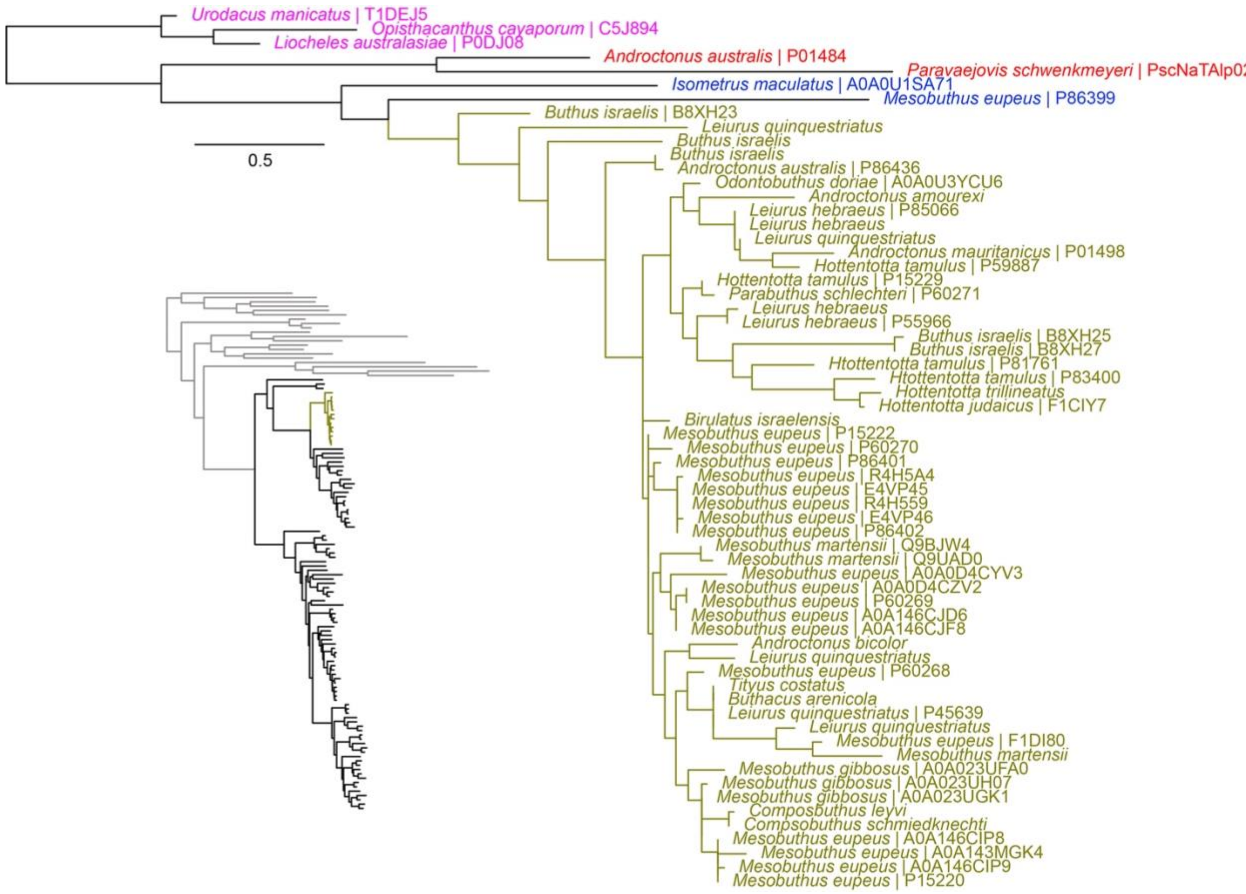

Supplementary Figure S12. Maximum likelihood gene tree recovered from the analysis of 56 chloride channel toxin (ClTx) peptides and seven outgroups. ClTx are unique to buthid scorpions as shown on the inset scorpion phylogeny.

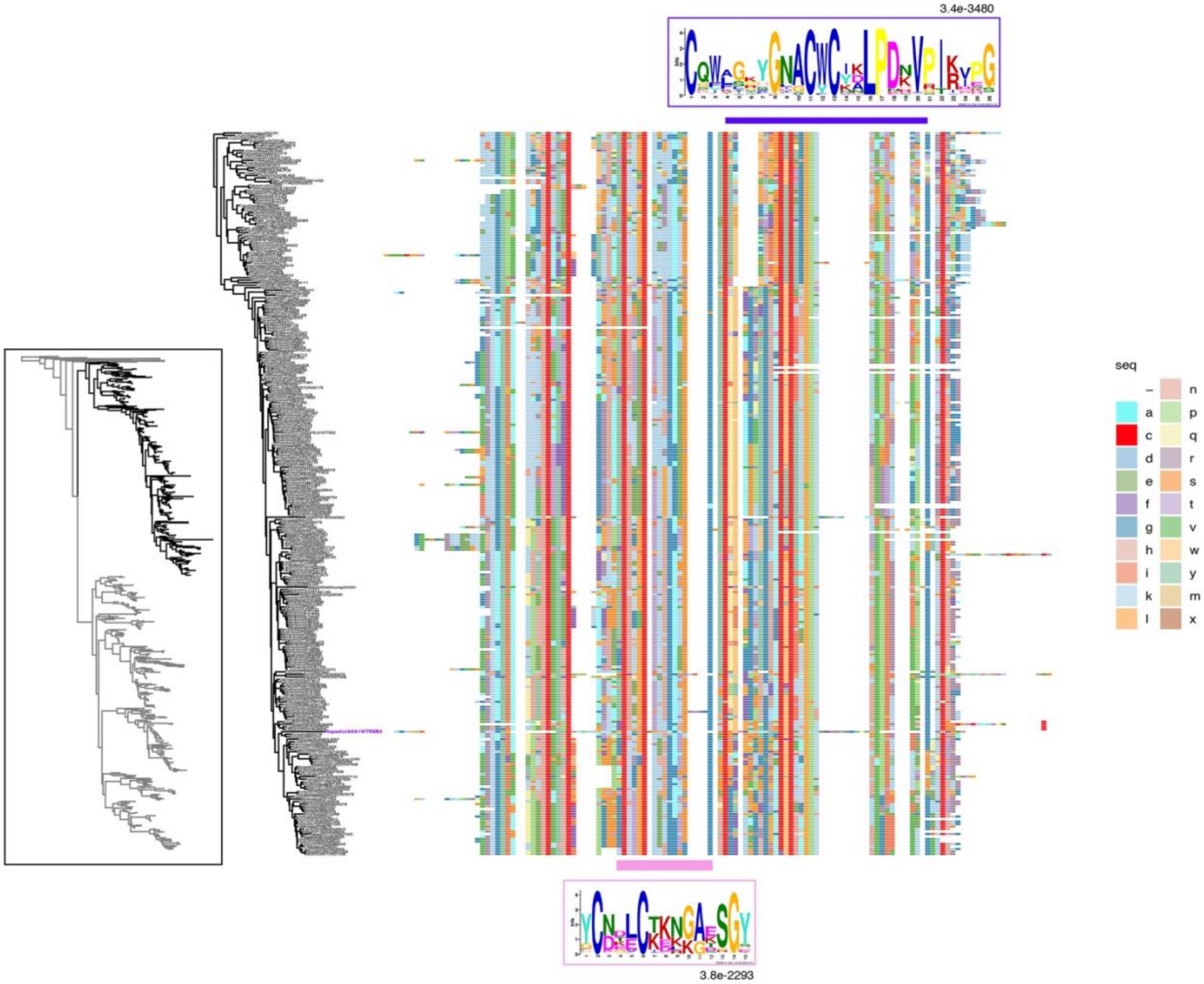

Supplementary Figure S13. Maximum likelihood gene tree recovered from the analysis of 723 Sodium channel toxin (NaTx) peptides recovered from our transcriptomic analyses and databases (UniProt and InterPro), plus two outgroups (inset). Multiple sequence alignment color-coded for the 294 peptides from the Aah2-like clade (highlighted in black on inset phylogeny). Mature peptide repetitive motifs found using Multiple Em for Motif Elicitation (MEME) locations as shown by colored bars.

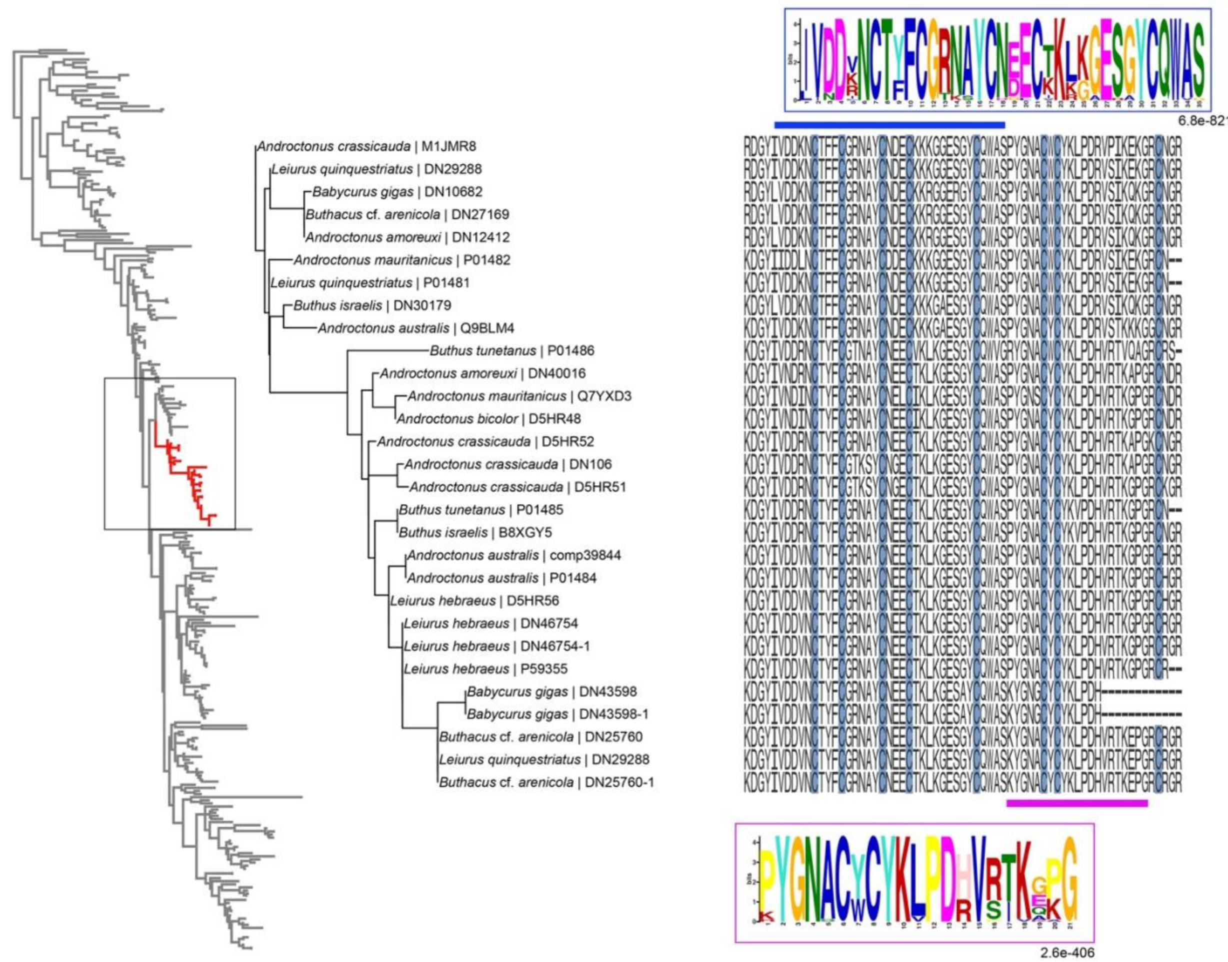

Supplementary Figure S14. Left: Pruned gene tree of the Aah2-like clade consisting of species from the *Buthus* group. Two sequences from *Babycurus gigas* might be cross contamination from the Trinity assembly (see their high similarity to other sequences from toxic species). Right: Multiple sequence alignment of the mature peptide showing the repetitive motifs found using Multiple Em for Motif Elicitation (MEME).

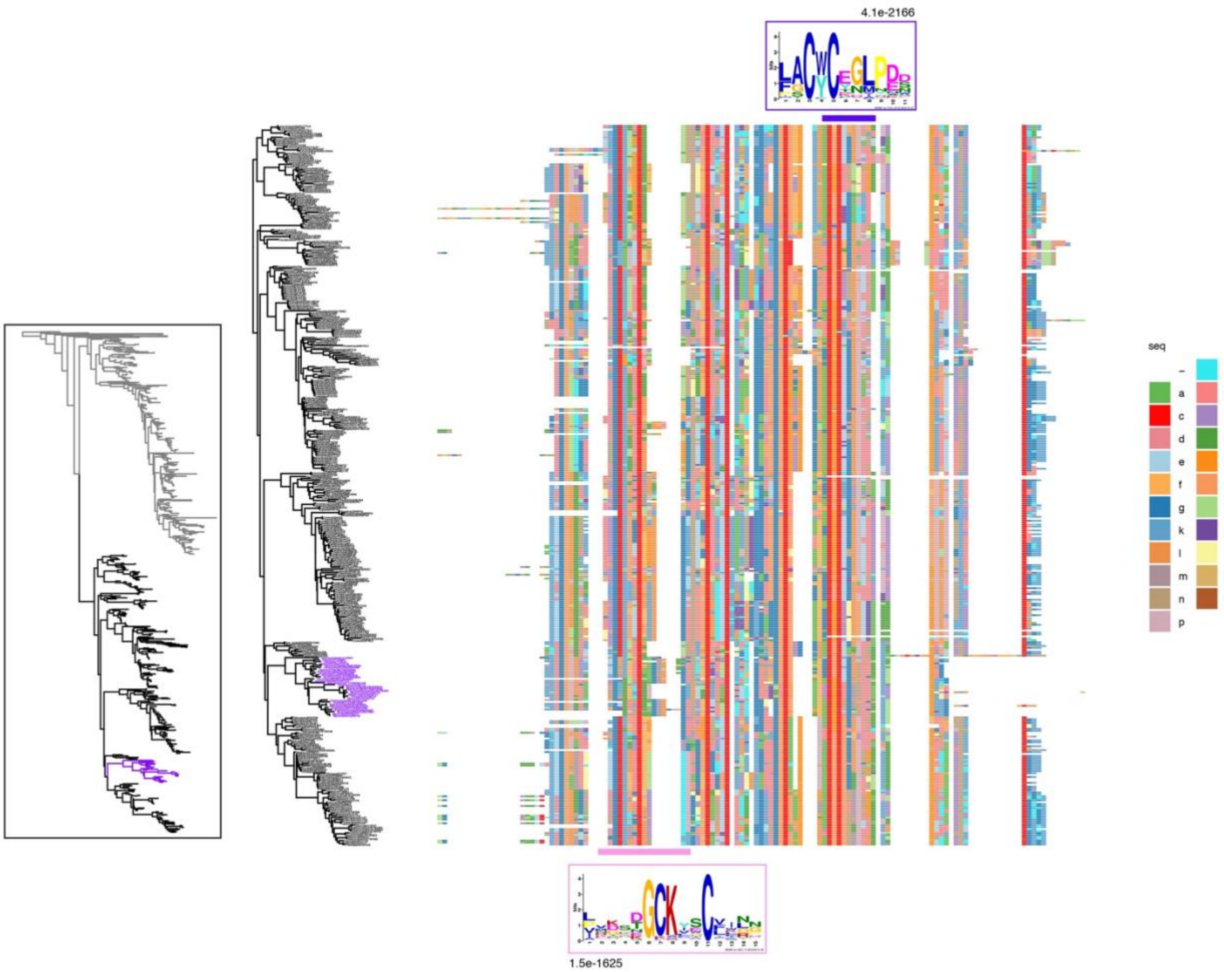

Supplementary Figure S15. Maximum likelihood gene tree recovered from the analysis of 723 sodium channel toxin (NaTx) peptides recovered from our transcriptomic analyses and databases (UniProt and InterPro), plus two outgroups (inset). Multiple sequence alignment color-coded for the 376 peptides from the Cn2-like clade (highlighted in black on inset phylogeny). Mature peptide repetitive motifs found using Multiple Em for Motif Elicitation (MEME) locations as shown by colored bars. Highlighted in purple is the sole clade of iurid scorpion Cn2-like peptides.

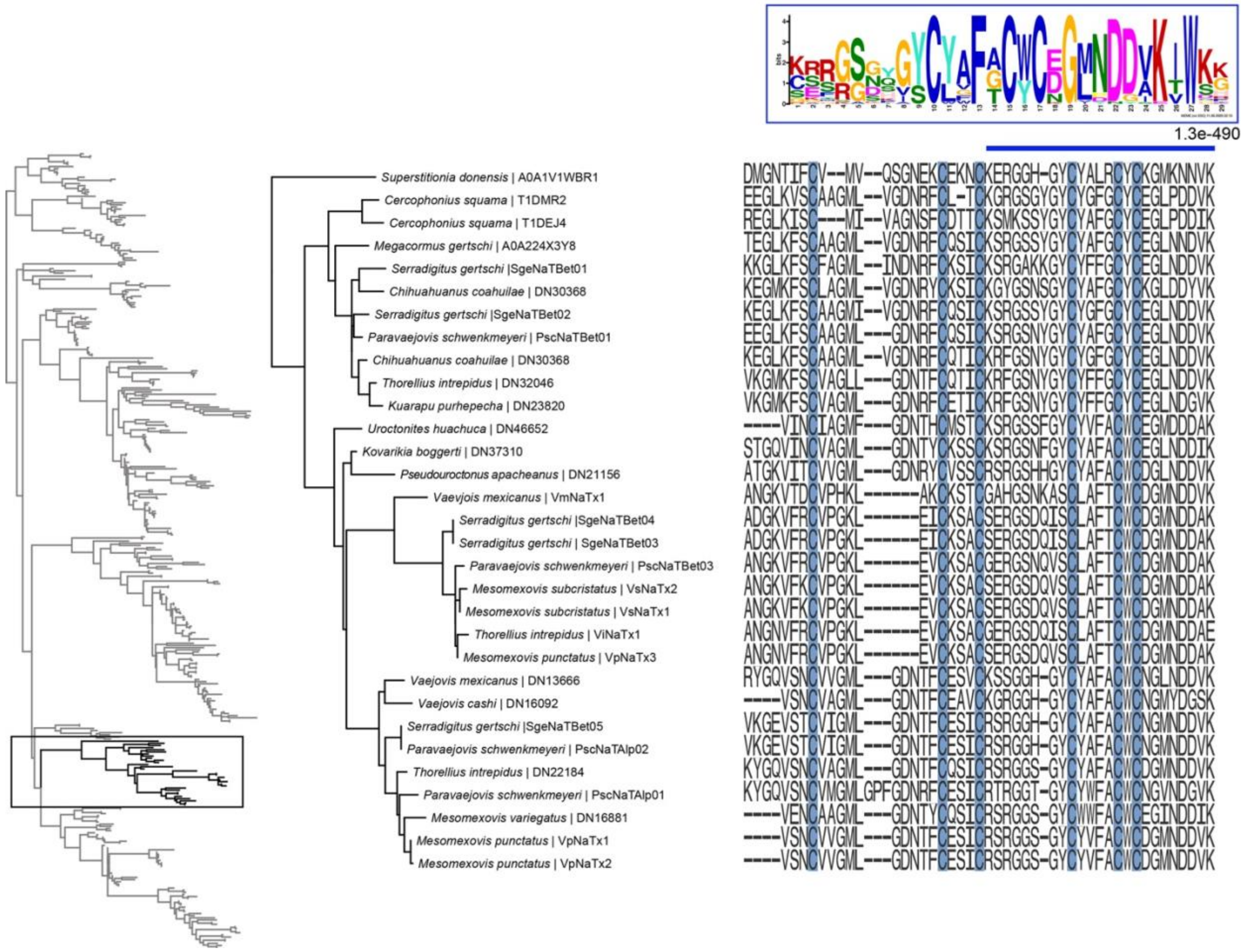

Supplementary Figure S16. Left: Pruned gene tree of the Cn2-like clade unique to Iurida. Right: Multiple sequence alignment of the mature peptide showing the repetitive motifs found using Multiple Em for Motif Elicitation (MEME).

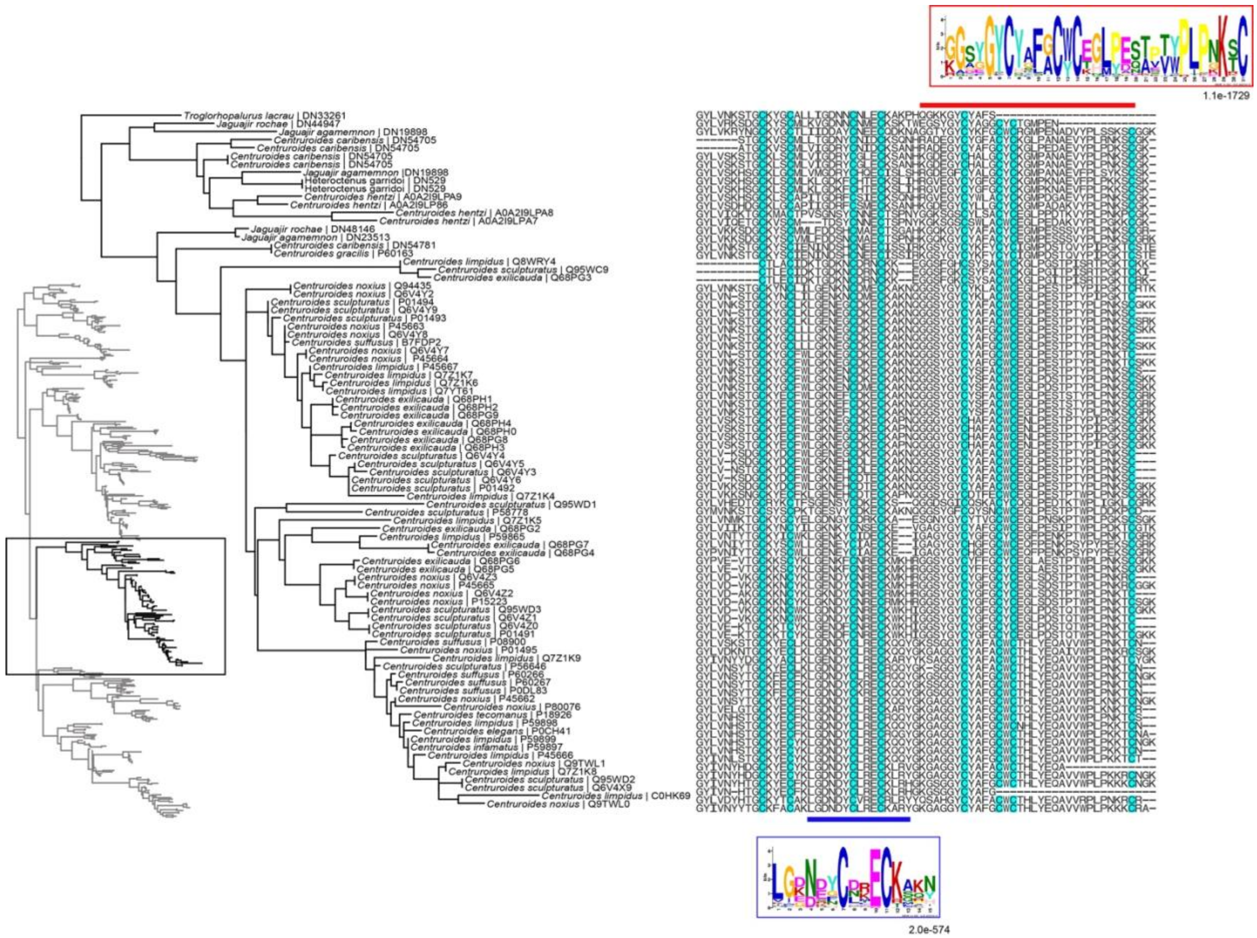

Supplementary Figure S17. Left: Pruned gene tree of the Cn2-like clade unique to the *Tityus* group, with emphasis on the genus *Centruroides*. Right: Multiple sequence alignment of the mature peptide showing the repetitive motifs found using Multiple Em for Motif Elicitation (MEME).

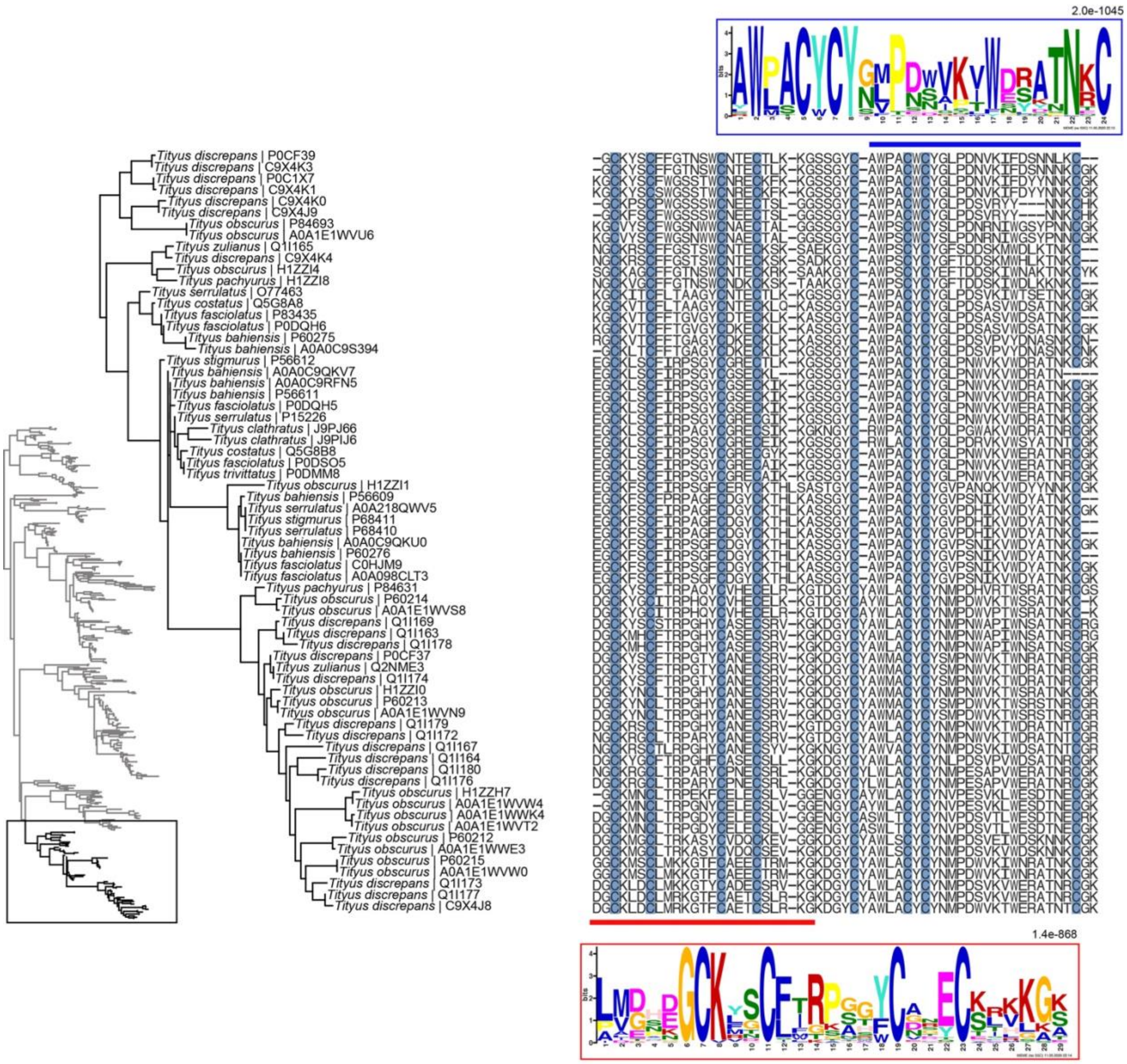

Supplementary Figure S18. Left: Pruned gene tree of the Cn2-like clade unique to the genus *Tityus*. Right: Multiple sequence alignment of the mature peptide showing the repetitive motifs found using Multiple Em for Motif Elicitation (MEME).

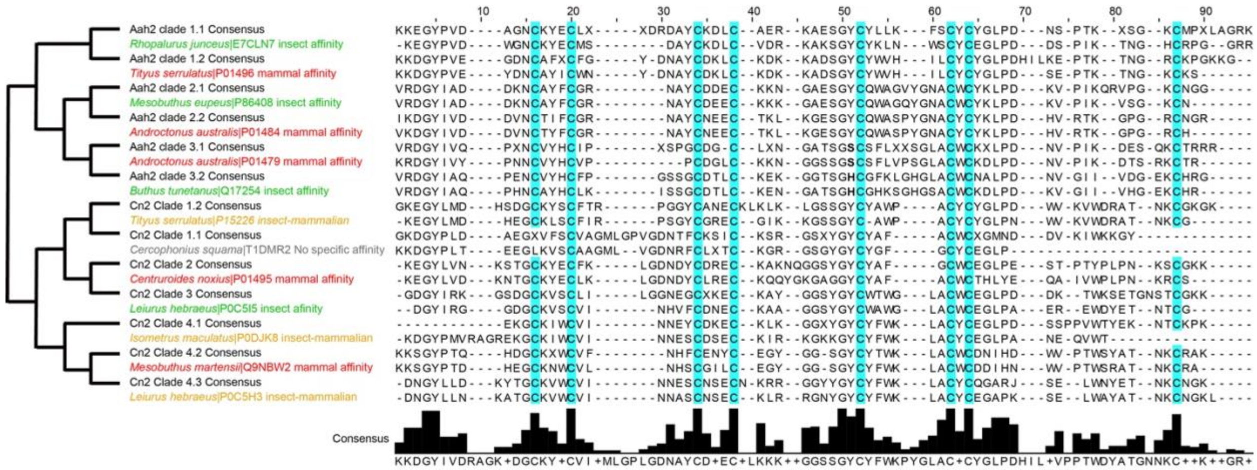

Supplementary Figure S19. Left: Comparative analysis of the consensus clades containing at least one peptide sequence with known function shown as function of their phylogenetic relationships. Right: Multiple sequence alignment of the consensus sequence (in black) and a representative sequence from that clade with known function. Green text: insect affinity; orange text: insect and mammal affinity; red text: mammal affinity.

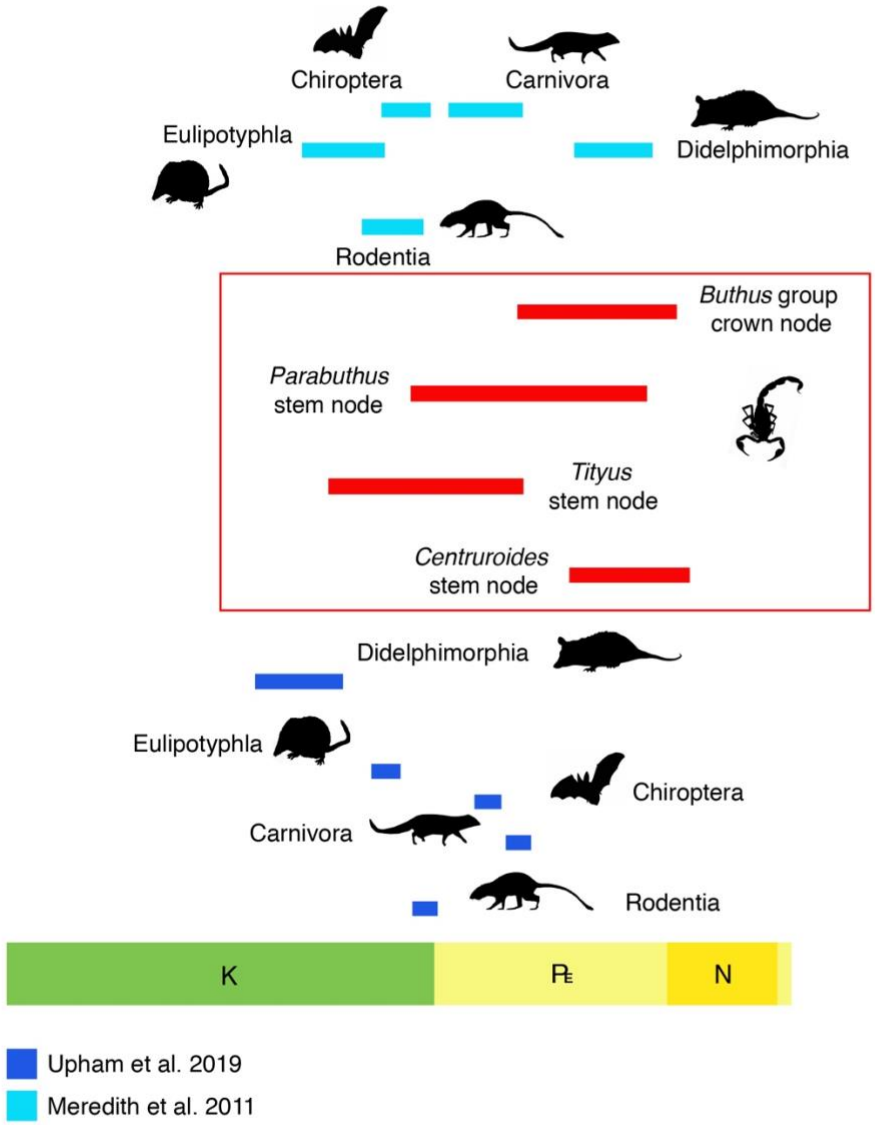

Supplementary Figure S20. 95% credibility intervals from our mammal-active toxin origins (in red), compared to 95% credibility intervals of the four major mammal orders that include scorpion predators, as shown by Meredith et al. (2011) and Upham et al. (2019).

Table S1. List of 100 scorpion species and 20 outgroup taxa included in phylogenomic analyses.

Order	Family	Species	Datatype	Accession
Outgroup				
Amblypygi	Charinidae	*Sarax israelensis*	SRA	PRJNA649577
	Phrynichidae	*Damon variegatus*	SRA	SRR1145694
Araneae	Theraphosidae	*Aphonopelma hentzi*	SRA	SRX10000054-5
	Tetragnathidae	*Leucauge venusta*	SRA	SRR1145740
	Liphistiidae	*Liphistius malayanus*	SRA	SRR1145736
Opiliones	Acropsopilionidae	*Acropsopilio neozealandiae*	SRA	SRR5235984
	Caddidae	*Caddo agilis*	SRA	SAMN06309539
	Phalangiidae	*Phalangium opilio*	SRA	SRX450969
	Sironidae	*Siro boyerae*	SRA	SRR1145699
	Taracidae	*Hesperonemastoma modestum*	SRA	SRR1145728
	Zalmoxidae	*Pachylicus acutus*	SRA	SRR1146670
Pseudoscorpiones	Chernetidae	*Hesperochernes* sp.	SRA	SRR1514877
	Feaellidae	*Feaella capensis*	SRA	SRR9331986
	Garypidae	*Synsphyronus apimelus*	SRA	SRR1145733
	Pseudotyrannochthoniidae	*Pseudotyrannochthonius* sp.	SRA	SRR9331998
Schizomida	Hubbardiidae	*Stenochrus portoricensis*	SRA	SRR6997625
Thelyphonida	Thelyphonidae	*Mastigoproctus giganteus*	SRA	SRR1145698
Xiphosura	Limulidae	*Limulus polyphemus*	SRA	SRR1145732
	Limulidae	*Carcinoscorpius rotundicauda*	SRA	SRX503911
	Limulidae	*Tachypleus tridentatus*	SRA	SRX5091311
Ingroup				
Scorpiones	Belisariidae	*Belisarius xambeui*	SRA	SRR1721953
	Bothriuridae	*Bothriurus burmeistei*	SRA	SRR1721670
		Bothriurus coriaceaus	SRA	SRR6467511
		Centromachetes sp.	SRA	SRR6467879
		Cercophonius sulcatus	SRA	SRR6466561
		Cercophonius squama	SRA	SRR6470146
		Cercophonius queenslandae	SRA	SRR6470446
	Buthidae	*Androctonus amoreuxi*	SRA	SAMN09939440
		Androctonus australis	SRA	SRR1724216
		Androctonus crassicauda	SRA	SAMN23426188
		Ananteris balzani	SRA	SAMN09907396
		Babycurus gigas	SRA	SAMN23426189
		Birulatus israelensis	SRA	SAMN23426190
		Buthacus cf. *arenicola*	SRA	SAMN23426191
		Buthus israelis	SRA	SAMN23426192
		Centruroides caribensis	SRA	SAMN23426193
		Centruroides sculpturatus	SRA	SRR1515193
		Centruroides vittatus	SRA	SRP035925
		Compsobuthus levyi	SRA	SAMN23426194
		Compsobuthus schmiedknechti	SRA	SAMN23426195
		Compsobuthus sp.	SRA	SAMN23426196
		Grosphus grandidieri	SRA	SAMN23426197
		Heteroctenus garridoi	SRA	SAMN23426198
		Heteroctenus junceus	SRA	SAMN23426199

	Hottentotta trilineatus	SRA	SRR1721800
	Jaquajir agamemnon	SRA	SAMN23426200
	Jaquajir rochae	SRA	SAMN23426201
	Leiurus hebraeus	SRA	SAMN23426202
	Leiurus quinquestriatus	SRA	SAMN23426203
	Lychas variatus	SRA	SAMN23426204
	Orthochirus scrobiculosus	SRA	SAMN23426205
	Parabuthus transvaalicus	SRA	SRR1721799
	Physoctonus debilis	SRA	SAMN23426206
	Tityus costatus	SRA	SAMN23426207
	Tityus maranhensis	SRA	SAMN23426208
	Tityus smithi	SRA	SAMN23426209
	Troglorhopalurus lacrau	SRA	SAMN23426210
	Uroplectes olivaceus	SRA	SAMN23426211
	Uroplectes vittatus	SRA	SAMN23426212
Caraboctonidae	*Caraboctonus keyserlingii*	SRA	SRR9053016
Chaeriliidae	*Chaerilus celebensis*	SRA	SRR1721804
Chactidae	*Anuroctonus phaiodactylus*	SRA	SRR1721879
	Brotheas granulatus	SRA	SRR1721887
Diplocentridae	*Diplocentrus diablo*	SRA	SRR1721672
	Diplocentrus zacatecanus	SRA	SAMN23438342
	Kolotl magnus	SRA	SRR7879236
	Kolotl poncei	SRA	SAMN23438343
	Nebo hierichonticus	SRA	SAMN23438341
Euscorpiidae	*Euscorpius italicus*	SRA	SRR1721892
	Megacormus gertschi	SRA	SRR3657526
	Megacormus sp.	SRA	SRR1767669
	Plesiochactas dilutus	SRA	SRR7250103
Hadruridae	*Hadrurus arizonensis*	SRA	SRR1721733
	Hadrurus concolorous	SRA	ERR3561754
	Hadrurus spadix	SRA	SRR4069278
	Hoffmannihadrurus aztecus	SRA	ERR3534794
Hormuridae	*Chiromachus ochropus*	SRA	SAMN23438348
	Hadogenes cf. *paucidens*	SRA	SAMN23438345
	Hadogenes troglodytes	SRA	SRR1721665
	Hormiops davidovi	SRA	SAMN23438338
	Hormurus waigiensis	SRA	SRR18036348
	Iomachus politus	SRA	SAMN23438344
	Liocheles australasiae	SRA	SRR1721664
	Liocheles sp.	SRA	SAMN23438340
	Opisthacanthus cf. *asper*	SRA	SAMN23438346
	Opisthacanthus validus	SRA	SAMN23438347
	Opisthacanthus madagascariensis	SRA	SRR1721668
	Palaeocheloctonus pauliani	SRA	SAMN23438349
Iuridae	*Iurus dekanum*	SRA	SRR1721734
Pseudochactidae	*Troglokhammouanus steineri*	SRA	SRR1721739
	Vietbocap lao	SRA	SRR1721740
Scorpiopidae	*Scorpiops* sp.	SRA	SRR1767662
Scorpionidae	*Opistophthalmus* cf. *boehmi*	SRA	SAMN23438352

	Opistophthalmus cf. *glabrifrons*	SRA	SAMN23438350
	Opistophthalmus cf. *wahlbergii*	SRA	SAMN23438351
	Pandinus imperator	SRA	SRR1721600
	Scorpio fuscus	SRA	SRR7249741
Superstitioniidae	*Superstitionia donensis*	SRA	SRR1721951
Urodacidae	*Urodacus elongatus*	SRA	SRR7885472
	Urodacus planimanus	SRA	SAMN06114579
	Urodacus yaschenkoi	SRA	SRR1557168
Vaejovidae	*Chihuahuanus coahuilae*	SRA	SRR7439185
	Konetontli acapulco	SRA	SRR7422029
	Konetontli chamelaensis	SRA	SRR7427084
	Kovarikia bogerti	SRA	SRR8518584
	Kuarapu purhepecha	SRA	SRR7439043
	Mesomexovis occidentalis	SRA	SRR7439610
	Mesomexovis aff. *variegatus*	SRA	SRR7439652
	Paravaejovis schwenkmeyeri	SRA	SRR2653951
	Paravaejovis spinigerus	SRA	SRR1721954
	Paruroctonus baergi	SRA	SRR7443668
	Pseudouroctonus apacheanus	SRA	SRR8518585
	Serradigitus gertschi	SRA	ERR2843384
	Smeringurus mesaensis	SRA	SRR7473845
	Smeringurus vachoni	SRA	SRR7474136
	Thorellius intrepidus	SRA	SRR7427141
	Uroctonites huachuca	SRA	SRR8518582
	Vaejovis cashi	SRA	SRR8518583
	Vaejovis mexicanus	SRA	SRR7421527
incertae sedis	*Uroctonus mordax*	SRA	SRR8518581

Table S2. Collecting localities of newly sequenced scorpions.

Species	Locality / Region of origin	Latitute	Longitude	Date	Collector
Ananteris balzani	Brazil: São Paulo State, Aguas de Sant Bárbara	-22.84	-49.35	V.2017	R. Pinto da Rocha
Androctonus amoreuxi	Israel: Haluza Sand dunes, East of Be'er Milka	30.93	34.41	31.vii.2017	C. Shlomo
Androctonus crassicauda	Israel: Entrance to Susita National Park, hand collecting and black-lighting at night	35.66362	32.77397		E. Gavish-Regev, S. Aharon, I. Armiach, J.A. Ballesteros, G. Gainett, P. Sharma
Babycurus gigas	USA: North Carolina	n/a	n/a	iv.2018	Captive bred (source colony B. Myers)
Birulatus israelensis	Israel: Mehola, Giv'at Sal'it Outside trail	32.36	35.51	7.v.2018	Y. Zvik
Buthacus cf. *arenicola*	Egypt: Senai, El Maghara	n/a	n/a	5/28/18	M. Kamel
Buthus israelis	Israel: Haluqim Ridge, West of Midreshet Ben-Gurion	30.85	34.76	16.VI.2017	E. Gavish-Regev & P. Sharma
Centruroides caribensis	USA: North Carolina	n/a	n/a	1.iii.2017	Captive bred (source colony B. Myers)
Chiromachus ochropus	Seychelles: Fregate Island	n/a	n/a	16.vii.2008	L. Monod
Compsobuthus levyi	Israel: Qanna'im Wadi near Arad	31.30	35.31	22.IX.2017	Y. Zvik
Compsobuthus schmiedknechti	Israel: Nahal Ktalav	31.73	35.07	19.VI.2017	E. Gavish-Regev & P. Sharma
Compsobuthus sp.	Israel: north to Rotem	32.34	35.52	4.vii.2016	Y. Zvik
Diplocentrus zacatecanus	Mexico: Zacatecas: Municipio Genaro Codina, 3 km SW de Genaro Codina	22.47	-102.48	2.ii.2017	P. Cushing, H. Carmona, E. González-Santillán
Grosphus grandidieri	Madagascar: ex-Province de Toamasina, Région Atsinana, Réserve Nat. Intégrale de Betampona	-17.91	49.18	11/16/15	S. Goodman
Hadogenes cf. *paucidens*	Tanzania	n/a	n/a	n/a	Captive bred (source colony L. Monod)
Heteroctenus garridoi	Cuba	n/a	n/a	n/a	Captive bred (source colony P. Sharma)
Heteroctenus junceus	Cuba	n/a	n/a	n/a	Captive bred (source colony B. Myers)
Hormiops davidovi	Vietnam: Con Son Island	n/a	n/a	8.i.2012	L. Monod
Hormurus waigiensis	Indonesia: Sulawesi Tengah, Pulau Peleng	n/a	n/a	16.iv.2013	L. Monod
Iomachus politus	Tanzania	n/a	n/a	n/a	Captive bred (source colony L. Monod)
Jaquajir agamemnon	Brazil: Piaui State, Castelo do Piauí	-5.32	-41.55	23.iii.2018	R. Pinto da Rocha
Jaquajir rochae	Brazil: Piaui State, Castelo do Piauí	-5.32	-41.55	23.iii.2018	R. Pinto da Rocha
Kolotl poncei	Mexico: Michoacan, Minicipio la Huacana, km 17 carretera Zicuiaran-Churumuco	18.81	-101.92	16.v.2015	E. Oliveros, J. Ponce-Saavedra, A. Quijano, J. Maldonado, E. González-Santillán
Leiurus hebraeus		30.99	34.89	5.viii.2016	Y. Zvik

	Israel: 100 meter north to Yeruham Lake , on ridge				
Leiurus quinquestriatus	Egypt	n/a	n/a	n/a	Captive bred (source colony E. Gavish-Regev)
Liocheles sp.	Thailand: Prachuap Khiri Khan Province	n/a	n/a	25.xii.2012	L. Monod
Lychas variatus	Australia: Queensland	21.13297	148.49246	27.v.2015	P. Sharma
Nebo hierichonticus	Israel:	n/a	n/a	n/a	Captive bred (source colony E. Gavish-Regev)
Opisthacanthus cf. *asper*	Tanzania	n/a	n/a	n/a	Captive bred (source colony L. Monod)
Opisthacanthus validus	South Africa	n/a	n/a	n/a	Captive bred (source colony L. Monod)
Opistophthalmus cf. boehmi	Tanzania	n/a	n/a	n/a	Captive bred (source colony L. Monod)
Opistophthalmus cf. glabrifrons	Mozambic	n/a	n/a	n/a	Captive bred (source colony L. Monod)
Opistophthalmus cf. wahlbergii	Mozambic	n/a	n/a	n/a	Captive bred (source colony L. Monod)
Orthochirus scrobiculosus	Israel: Haluqim Ridge, West of Midreshet Ben-Gurion	30.85	34.76	16.VI.2017	E. Gavish-Regev & P. Sharma
Palaeocheloctonus pauliani	Madagascar	n/a	n/a	n/a	Captive bred (source colony L. Monod)
Physoctonus debilis	Brazil: Piaui State, Castelo do Piauí	-5.32	-41.55	23.iii.2018	R. Pinto da Rocha
Tityus costatus	Brazil: São Paulo State	n/a	n/a	2017	R. Pinto da Rocha
Tityus maranhensis	Brazil: Ceará State, Ubajara (Pousada Sítio do Alemão)	-3.73	-40.90	24.iii.2018	R. Pinto da Rocha
Tityus smithi	USA: North Carolina	n/a	n/a	n/a	Captive bred (source colony B. Myers)
Troglorhopalurus lacrau	Brazil: Bahia State, Itaeté (Lapa do Bode)	-12.98	-40.97	22.iii.2017	R. Pinto da Rocha
Uroplectes olivaceus	USA: North Carolina	n/a	n/a	n/a	Captive bred (source colony B. Myers)
Uroplectes vittatus	USA: North Carolina	n/a	n/a	n/a	Captive bred (source colony B. Myers)

Table S3. Readouts and accession data for 42 scorpion species newly sequenced in this study.

	Species	Reads	Contigs	Method
BUTHOIDEA				
Buthidae	*Androctonus amoreuxi*	19078891	56289	HiSeq 2 X 150
	Androctonus crassicauda	22416824	23683	HiSeq 2 X 150
	Ananteris balzani	22362527	83351	HiSeq 2 X 150
	Babycurus gigas	16376118	5913	HiSeq 2 X 150
	Birulatus israelensis	50794420	71390	HiSeq 2 X 150
	Buthacus cf. *arenicola*	19804050	65727	HiSeq 2 X 150
	Buthus israelis	62601743	31901	HiSeq 2 X 150
	Centruroides caribensis	16971304	77404	HiSeq 2 X 150
	Compsobuthus levyi	18633893	73168	HiSeq 2 X 150
	Compsobuthus schmiedknechti	76433324	59310	HiSeq 2 X 150
	Compsobuthus sp.	61356146	55775	HiSeq 2 X 150
	Grosphus grandidieri	33078770	68375	HiSeq 2 X 150
	Heteroctenus garridoi	25401187	80482	HiSeq 2 X 150
	Heteroctenus junceus	30459300	167545	HiSeq 2 X 150
	Jaquajir agamemnon	19088930	48581	HiSeq 2 X 150
	Jaquajir rochae	14969285	40854	HiSeq 2 X 150
	Leiurus hebraeus	18235433	50196	HiSeq 2 X 150
	Leiurus quinquestriatus	17163687	63331	HiSeq 2 X 150
	Lychas variatus	16471150	84008	HiSeq 2 X 150
	Orthochirus scrobiculosus	31849129	32859	HiSeq 2 X 150
	Physoctonus debilis	12895814	12062	HiSeq 2 X 150
	Tityus costatus	17843661	69201	HiSeq 2 X 150
	Tityus maranhensis	16247484	62184	HiSeq 2 X 150
	Tityus smithi	19198142	78192	HiSeq 2 X 150

	Troglorhopalurus lacrau	16104040	65928	HiSeq 2 X 150
	Uroplectes olivaceus	19657025	71864	HiSeq 2 X 150
	Uroplectes vittatus	19980384	245104	HiSeq 2 X 150
SCORPIONOIDEA				
Diplocentridae	*Diplocentrus zacatecanus*	64264547	141792	HiSeq 2 X 150
	Kolotl poncei	25294080	105290	HiSeq 2 X 150
	Nebo hierichonticus	40511893	647989	HiSeq 2 X 150
Hormuridae	*Chiromachus ochropus*	25719159	249450	HiSeq 2 X 150
	Hadogenes paucidens	26367367	140326	HiSeq 2 X 150
	Hormiops davidovi	27660036	378177	HiSeq 2 X 150
	Hormurus waigiensis	20560984	287004	HiSeq 2 X 150
	Iomachus politus	23055924	300022	HiSeq 2 X 150
	Liocheles sp.	18600474	86885	HiSeq 2 X 150
	Opisthacanthus cf. *asper*	24099159	513757	HiSeq 2 X 150
	Opisthacanthus validus	16652215	252340	HiSeq 2 X 150
	Palaeocheloctonus pauliani	9955624	267572	HiSeq 2 X 150
Scorpionidae	*Opistophthalmus* cf. *boehmi*	40823006	60020	HiSeq 2 X 150
	Opistophthalmus cf. *glabrifrons*	34221314	305201	HiSeq 2 X 150
	Opistophthalmus cf. *wahlbergii*	22341990	265140	HiSeq 2 X 150

Table S4. Accession data for 21 scorpion species, plus other Sanger-sequenced datasets, added to phylogenetic analyses to tests generic groupings within Buthidae (“M2plus”).

	Species	Datatype	Accession	18S rRNA	COI	16S rRNA
BUTHOIDEA						
Buthidae	*Anateris balzani*	SRA	see Table S1	From transcriptome	KY674491	KY674448
	Babycurus gigas	SRA	see Table S1	From transcriptome	Not available	Not available
	Androctonus amoreuxi	SRA	see Table S1	From transcriptome	KJ538492	AY226175
	Androctonus australis	SRA	see Table S1	From transcriptome	AF370829	KJ538473
	Androctonus crassicauda	SRA	see Table S1	From transcriptome	HM567333	FJ217735
	Androctonus mauritanicus	SRA	PRJNA556947	From transcriptome	Not available	Not available
	Apistobuthus pterygocercus	Sanger	-	Not available	Not available	AY226178
	Birulatus israelensis	SRA	see Table S1	From transcriptome	Not available	Not available
	Buthacus cf. *arenicola*	SRA	see Table S1	From transcriptome	Not available	Not available
	Buthus israelensis	SRA	see Table S1	From transcriptome	Not available	Not available
	Compsobuthus levyi	SRA	see Table S1	From transcriptome	Not available	Not available
	Hottentotta gentilli	SRA	PRJNA556947	From transcriptome	JF820093	JQ514227
	Hottentotta trilineatus	SRA	see Table S1	From transcriptome	Not available	Not available
	Kraepelinia palpator	Sanger	-	Not available	Not available	AY226181
	Leiurus hebraeus	SRA	see Table S1	From transcriptome	Not available	Not available
	Leiurus quinquestriatus	SRA	see Table S1	From transcriptome	JQ514258	AY226174
	Liobuthus kessleri	Sanger	-	Not available	MN071133	MN071126
	Mesobuthus gibbosus	EST	[1]	Not available	DQ310884	DQ310847
	Meosbuthus martensii	Genome	GCA_000484575.1	AB008465	JF700146	Not available
	Orthochirus scrobiculosus	SRA	see Table S1	From transcriptome	Not available	Not available
	Vachoniolus globimanus	Sanger	-	Not available	Not available	AY226179
	Australobuthus xerolimniorum	SRA	SRR870659	Not available	Not available	Not available
	Isometroides vescus	SRA	SRR870661	Not available	Not available	Not available

	Lychas buchardi	SRA	SRR870662	Not available	Not available	Not available
	Lychas mucronatus	Sanger	-	JN018270	JN018153	AF370855
	Lychas variatus	SRA	see Table S1	From transcriptome	Not available	Not available
	Charmus sp.	Sanger	-	Not available	MF422296	Not available
	Grosphus flavopiceus	Sanger	-	JN018269	JN018152	JQ514238
	Grosphus grandidieri	SRA	see Table S1	From transcriptome	Not available	Not available
	Parabuthus laevifrons	Sanger	-	JN018271	JN018154	Not available
	Centruroides hentzi	SRA	SRX3189905	AF062948	MK479177	Not available
	Tityus serrulatus	SRA	SRX708114	JN018272	JN018155	AY586781
Chaeriliidae	*Chaerilus julietteae*	Sanger	-	JN018280	JN018163	Not available
	Chaerilus sp.	Sanger	-	JN018279	JN018162	Not available
IUROIDEA						
Iuridae	*Protoiurus kraepelini*	SRA	PRJNA556947	Not available	Not available	Not available

[1] Diego-García, E., Caliskan, F. & Tytgat, J. 2014. The Mediterranean scorpion *Mesobuthus gibbosus* (Scorpiones, Buthidae): transcriptome analysis and organization of the genome encoding chlorotoxin-like peptides. BMC Genomics 15, 295

Table S5. Fossil calibrations used in molecular dating analyses. Ages in millions of years.

Node calibrated	Fossil	Minimum age	Maximum age	Reference
Root		none	550	Numerous
Opiliones (stem)	*Eophalangium sheari*	411	none	Garwood et al. 2014
Eupnoi (Caddo + Phalangium)	*Ameticos scolos*	305	none	Garwood et al. 2011
Dyspnoi (Acropsopilio + Hesperonemastoma)	*Macrogyion cronus*	305	none	Garwood et al. 2011
Araneae (stem)	*Attercopus fimbriunguis*	386	none	Selden et al. 2008, Huang et al. 2018
Amblypygi (stem)	Graeophonus anglicus, Graeophonus carbonarius	312	none	Pocock 1911
Thelyphonida (stem)	*Prothelyphonus naufraga*	319	none	Brauckmann and Kock 1983
Liphistiidae	*Palaeothele montceauensis*	305	none	Selden 1996
Xiphosura (stem)	*Lunataspis aurora*	445	none	Rudkin et al. 2008
Pseudoscorpiones (stem)	*Dracochela deprehendor*	392	none	Schawaller et al. 1991
Scorpiones (stem)	*Dolichophonus loudenensis*, *Eramoscorpius brucensis*	435.15	514	Laurie 1899
Scorpiones (crown)	*Protoischnurus axelrodurum*, *Compsoscorpius buthiformis*	112.6	313.7	de Carvalho and Lourenço 2001; Menon 2007
Iurida (stem)	*Protoischnurus axelrodurum*, *Compsoscorpius buthiformis*	112.6	313.7	de Carvalho and Lourenço 2001; Menon 2007
Chaerilidae (stem)	*Electrochaerilus buckleyi*	98.17	313.7	Santiago-Blay 2004; Soleglad et al. 2004a
Buthoidea (crown)	*Uintascorpio halandrasi*	49.26	313.7	Perry 1995, Soleglad et al. 2004b
Scorpionoidea (crown)	*Compsoscorpius buthiformis*	112.6	313.7	Pointon et al. 2012

References (in order of appearance)

Garwood, R. J., Sharma, P. P., Dunlop, J. A., & Giribet, G. (2014). A Paleozoic stem group to mite harvestmen revealed through integration of phylogenetics and development. Current Biology, 24(9), 1017-1023.

Garwood, R. J., Dunlop, J. A., Giribet, G., & Sutton, M. D. (2011). Anatomically modern Carboniferous harvestmen demonstrate early cladogenesis and stasis in Opiliones. Nature Communications, 2(1), 1-7.

Selden, P. A., Shear, W. A., & Sutton, M. D. (2008). Fossil evidence for the origin of spider spinnerets, and a proposed arachnid order. Proceedings of the National Academy of Sciences, 105(52), 20781-20785.

Huang, D., Hormiga, G., Cai, C., Su, Y., Yin, Z., Xia, F., & Giribet, G. (2018). Origin of spiders and their spinning organs illuminated by mid-Cretaceous amber fossils. Nature ecology & evolution, 2(4), 623-627.

Pocock, R.I. (1911). A monograph of the terrestrial Carboniferous Arachnida of Great Britain. Monographies Palaeontographical Society, 64:1–84.

Brauckmann, C., & Koch, L. (1983). *Prothelyphonus naufragus* n. sp., ein neuer Geisselskorpion [Arachnida: Thelyphonida: Thelyphonidae] aus dem Namurium unteres Oberkarbon) von West-Deutschland. Entomologica Germania, 9, 63-74.

Selden, P. A. (1996). First fossil mesothele spider, from the Carboniferous of France.

Rudkin, D. M., Young, G. A., & Nowlan, G. S. (2008). The oldest horseshoe crab: a new xiphosurid from Late Ordovician Konservat-Lagerstätten deposits, Manitoba, Canada. Palaeontology, 51(1), 1-9.

Schawaller, W., Shear, W. A., & Bonamo, P. M. (1991). The first Paleozoic pseudoscorpions (Arachnida, Pseudoscorpionida). American museum novitates (USA).

Laurie, M. (1900). XIX.—On a Silurian Scorpion and some additional Eurypterid Remains from the Pentland Hills. Earth and Environmental Science Transactions of The Royal Society of Edinburgh, 39(3), 575-590.

Maria da Gloria, P., & Lourenço, W. R. (2001). A new family of fossil scorpions from the Early Cretaceous of Brazil. Comptes Rendus de l'Académie des Sciences-Series IIA-Earth and Planetary Science, 332(11), 711-716.

Menon, F. (2007). Higher systematics of scorpions from the Crato Formation, Lower Cretaceous of Brazil. Palaeontology, 50(1), 185-195.

Santiago-Blay, J. A. (2004). *Electrochaerilus* (Scorpiones: Chaerilidae): Another piece in the mesozoic scorpion puzzle. Denver Annual Meeting.

Soleglad, M. E., Fet, V., & Blay, J. A. S. (2004a). A redescription and family placement of" Uintascorpio" Perry, 1995 from the Parachute Creek Member of the Green River Formation (Middle Eocene) of Colorado, USA (Seorpiones: Buthidae). Revista ibérica de aracnología, (10), 7-16.

Perry, M. L. (1995). Preliminary Description of a New Fossil Scorpion from the Middle Eocene, Green River Formation, Rio Blanco County, Colorado.

Soleglad, M. E., Fet, V., Anderson, S. R., & Blay, J. A. S. (2004b). A new genus and subfamily of scorpions from Lower Cretaceous Burmese amber (Scorpiones: Chaerilidae). Revista Ibérica de Aracnología, (9), 3-14.

Pointon, M. A., Chew, D. M., Ovtcharova, M., Sevastopulo, G. D., & Crowley, Q. G. (2012). New high-precision U–Pb dates from western European Carboniferous tuffs; implications for time scale calibration, the periodicity of late Carboniferous cycles and stratigraphical correlation. Journal of the Geological Society, 169(6), 713-721.

Table S6. Sequences of scorpion toxins retrieved from UniProt. Asterisks indicate peptides with known mammal affinity, with associated references.

Species	Class	UniProt accession number	References for mammal-active peptides
Opisthacanthus cayaporum	DDH	C5J894	
Hemiscorpius lepturus	DDH	A0A1L4BJ56	
Liocheles australasiae	DDH	P0DJ08	
Urodacus manicatus	DDH	T1DMR4	
Urodacus manicatus	DDH	T1DEJ5	
Urodacus manicatus	DDH	T1DPA2	
Opistophthalmus carinatus	Calcin	P60253	
Opistophthalmus carinatus	Calcin	P60252	
Pandinus imperator	Calcin	P59868	
Hemiscorpius lepturus	Calcin	A0A1L4BJ42	
Scorpio maurus	Calcin	P60254	
Megacormus gertschi	Calcin	A0A224X3Z6	
Megacormus gertschi	Calcin	A0A224X3X5	
Superstitionia donensis	Calcin	A0A1V1WBN6	
Superstitionia donensis	Calcin	A0A1V1WBN1	
Hoffmannihadrurus gertschi	Calcin	B8QG00	
Hadrurus spadix	Calcin	JAV48253	
Vaejovis mexicanus	Calcin	P0DPT1	
Thorellius intrepidus	Calcin	P0DM30	
Mesobuthus eupeus	ClTx	A0A146CIP8	
Mesobuthus eupeus	ClTx	A0A143MGK4	
Mesobuthus eupeus	ClTx	A0A146CIP9	
Mesobuthus eupeus	ClTx	P15220	
Mesobuthus gibbosus	ClTx	A0A023UGK1	
Mesobuthus gibbosus	ClTx	A0A023UH07	
Mesobuthus gibbosus	ClTx	A0A023UFA0	
Mesobuthus eupeus	ClTx	P60268	
Leiurus quinquestriatus	ClTx	P45639	
Mesobuthus eupeus	ClTx	A0A0D4CYV3	
Mesobuthus martensii	ClTx	Q9BJW4	
Mesobuthus martensii	ClTx	Q9UAD0	
Mesobuthus eupeus	ClTx	A0A146CJD6	
Mesobuthus eupeus	ClTx	A0A146CJF8	
Mesobuthus eupeus	ClTx	A0A0D4CZV2	
Mesobuthus eupeus	ClTx	F1DI80	
Mesobuthus eupeus	ClTx	P60269	
Mesobuthus eupeus	ClTx	P60270	
Androctonus australis	ClTx	P86436	

Buthus israelis	ClTx	B8XH25
Buthus israelis	ClTx	B8XH27
Hottentotta tamulus	ClTx	P81761
Hottentotta tamulus	ClTx	P83400
Hottentotta judaicus	ClTx	F1CIY7
Mesobuthus eupeus	ClTx	P15222
Mesobuthus eupeus	ClTx	P86401
Mesobuthus eupeus	ClTx	E4VP45
Mesobuthus eupeus	ClTx	E4VP46
Mesobuthus eupeus	ClTx	R4H559
Mesobuthus eupeus	ClTx	P86402
Mesobuthus eupeus	ClTx	R4H5A4
Leiurus hebraeus	ClTx	P55966
Hottentotta tamulus	ClTx	P15229
Parabuthus schlechteri	ClTx	P60271
Odontobuthus doriae	ClTx	A0A0U3YCU6
Leiurus hebraeus	ClTx	P85066
Androctonus mauritanicus	ClTx	P01498
Hottentotta tamulus	ClTx	P59887
Buthus israelis	ClTx	B8XH23
Lychas mucronatus	KTx	P0CI88
Isometrus maculatus	KTx	P0DJL0
Mesobuthus gibbosus	KTx	A0A059UHJ5
Hottentotta conspersus	KTx	JZ8220909
Hottentotta judaicus	KTx	F1CIZ6
Mesobuthus martensii	KTx	Q8I6X9
Tityus serrulatus	KTx	P0C175
Mesobuthus eupeus	KTx	P86399
Mesobuthus eupeus	KTx	P86399
Androctonus bicolor	KTx	A0A0K0LBY9
Buthus occitanus	KTx	B8XH22
Androctonus australisS	KTx	LKTx
Hoffmannihadrurus gertschi	KTx	Q0GY40
Heterometrus laoticus	KTx	P0DJ41
Mesobuthus eupeus	KTx	A0A088D9T9
Mesobuthus martensii	KTx	A7KJJ7
Buthus tunetanus	KTx	C0HJQ2
Mesobuthus eupeus	KTx	A0A088DAE2
Mesobuthus martensii	KTx	P83407
Centruroides tecomanus	KTx	C0HJW2

Lychas mucronatus	KTx	D9U2B0
Isometrus maculatus	KTx	A0A0U1SA71
Isometrus maculatus	KTx	A0A0U1S616
Isometrus maculatus	KTx	A0A0U1SK86
Chaerilus tricostatus	KTx	P0DJO5
Lychas mucronatus	KTx	P0CI47
Isometroides vescus	KTx	T1DMS1
Isometrus maculatus	KTx	A0A0U1SSR1
Buthus israelis	KTx	B8XH44
Isometrus maculatus	KTx	A0A0U1TYB8
Mesobuthus gibbosus	KTx	A0A059UEE4
Mesobuthus gibbosus	KTx	A0A059UHK0
Tityus obscurus	KTx	A0A1E1WVQ0
Tityus obscurus	KTx	A0A1E1WVW2
Tityus discrepans	KTx	P84777
Lychas mucronatus	KTx	D9U2A8
Buthus israelis	KTx	B8XH38
Mesobuthus eupeus	KTx	A0A088D9R3
Buthus israelis	KTx	B8XH43
Mesobuthus martensii	KTx	Q86BX0
Buthus israelis	KTx	B8XH37
Mesobuthus eupeus	KTx	A0A088DB08
Mesobuthus martensii	KTx	Q8I0L5
Androctonus amoreuxi	KTx	Q5K0E0
Mesobuthus eupeus	KTx	A0A143MGR2
Androctonus australis	KTx	Q86SD8
Androctonus australis	KTx	Q867F4
Androctonus australis	KTx	P60233
Androctonus mauritanicus	KTx	P60208
Isometrus maculatus	KTx	A0A0U1TYC6
Isometrus maculatus	KTx	P0CJ24
Isometrus maculatus	KTx	A0A0U1S4N0
Isometrus maculatus	KTx	A0A0U1TZ20
Isometrus maculatus	KTx	A0A0U1SCI3
Lychas mucronatus	KTx	A0A0U1S505
Lychas mucronatus	KTx	P0CH12
Isometrus maculatus	KTx	A0A0U1TZ12
Lychas mucronatus	KTx	P0CI48
Mesobuthus eupeus	KTx	A0A088D9S3
Androctonus mauritanicus	KTx	P31719

Mesobuthus martensii	KTx	Q9TVX3
Leiurus hebraeus	KTx	P16341
Hottentotta tamulus	KTx	P59869
Hottentotta tamulus	KTx	P59870
Orthochirus scrobiculosus	KTx	P55896
Buthus occitanus paris	KTx	P0DL44
Buthus israelis	KTx	B8XH29
Buthus israelis	KTx	P0C908
Hottentotta tamulus	KTx	P59886
Odontobuthus doriae	KTx	A0A0U4FP89
Odontobuthus doriae	KTx	P0C909
Buthus israelis	KTx	B8XH48
Leiurus hebraeus	KTx	P46110
Leiurus hebraeus	KTx	P46111
Leiurus hebraeus	KTx	P46112
Androctonus mauritanicus	KTx	P24662
Androctonus bicolor	KTx	A0A0K0LBX5
Androctonus amoreuxi	KTx	P0C8R1
Mesobuthus eupeus	KTx	P86396
Mesobuthus eupeus	KTx	C0HJQ6
Mesobuthus martensii	KTx	Q9NII7
Mesobuthus eupeus	KTx	A0A088D9R0
Androctonus bicolor	KTx	A0A0K0LBX7
Buthus tunetanus	KTx	P59290
Androctonus australis	KTx	P45696
Mesobuthus gibbosus	KTx	K7XFK5
Mesobuthus eupeus	KTx	A0A088D9R9
Mesobuthus eupeus	KTx	A0A088DB48
Mesobuthus eupeus	KTx	C0HJQ4
Centruroides suffusus	KTx	P85529
Centruroides tecomanus	KTx	C0HJW1
Centruroides elegans	KTx	P0C163
Centruroides limpidus	KTx	P45629
Centruroides elegans	KTx	P0C162
Centruroides noxius	KTx	P08815
Centruroides elegans	KTx	P0C161
Centruroides tecomanus	KTx	C0HJW6
Centruroides elegans	KTx	P0C164
Centruroides tecomanus	KTx	C0HJW5
Centruroides elegans	KTx	P0C165

Centruroides limpidus	KTx	P0DL70
Centruroides limpidus	KTx	P45630
Centruroides limbatus	KTx	P59847
Centruroides limbatus	KTx	P59850
Centruroides margaritatus	KTx	P40755
Centruroides limbatus	KTx	P59849
Heteroctenus junceus	KTx	C0HJT0
Heteroctenus garridoi	KTx	P0DL43
Centruroides hentzi	KTx	A0A2I9LNQ2
Centruroides hentzi	KTx	A0A2I9LNP3
Centruroides hentzi	KTx	A0A2I9LNQ1
Centruroides limbatus	KTx	P59848
Centruroides hentzi	KTx	A0A2I9LNQ6
Centruroides hentzi	KTx	A0A2I9LNP1
Centruroides noxius	KTx	Q9TXD1
Centruroides hentzi	KTx	A0A2I9LNP9
Tityus obscurus	KTx	A0A1E1WWJ8
Tityus bahiensis	KTx	A0A0C9S0L0
Tityus serrulatus	KTx	P56219
Tityus discrepans	KTx	P59925
Tityus obscurus	KTx	P60210
Parabuthus transvaalicus	KTx	P83112
Tityus stigmurus	KTx	P0CB56
Tityus serrulatus	KTx	P46114
Tityus stigmurus	KTx	P0DPT4
Tityus bahiensis	KTx	A0A0C9QKU6
Tityus costatus	KTx	Q5G8B6
Tityus serrulatus	KTx	A0A218QXG2
Tityus serrulatus	KTx	A0A218QX22
Tityus serrulatus	KTx	A0A218QWZ7
Tityus serrulatus	KTx	A0A218QWZ8
Tityus serrulatus	KTx	A0A218QXC2
Tityus costatus	KTx	P0C185
Tityus bahiensis	KTx	A0A0C9S3A0
Tityus serrulatus	KTx	A0A218QXB7
Tityus serrulatus	KTx	P59936
Tityus trivittatus	KTx	P0C168
Tityus stigmurus	KTx	P0C8L1
Mesobuthus martensii	KTx	P59938
Mesobuthus eupeus	KTx	A0A088DAE4

Mesobuthus eupeus	KTx	Q9BKB7
Mesobuthus martensii	KTx	V9LLY8
Mesobuthus eupeus	KTx	A0A143Q3Q3
Mesobuthus martensii	KTx	H2ER23
Mesobuthus martensii	KTx	Q9NII6
Mesobuthus martensii	KTx	A0RZD1
Mesobuthus eupeus	KTx	C0HJQ7
Mesobuthus eupeus	KTx	C0HJQ8
Mesobuthus martensii	KTx	H2ETQ6
Mesobuthus eupeus	KTx	A0A088DAD7
Mesobuthus martensii	KTx	H2ER22
Mesobuthus martensii	KTx	Q1EFP8
Mesobuthus martensii	KTx	Q9NII5
Hottentotta judaicus	KTx	F1CJ83
Hottentotta tamulus	KTx	P24663
Centruroides noxius	KTx	P0C182
Heteroctenus junceus	KTx	C0HJS9
Centruroides limbatus	KTx	P0C167
Leiurus hebraeus	KTx	P45628
Leiurus hebraeus	KTx	P59943
Leiurus hebraeus	KTx	P59944
Leiurus hebraeus	KTx	P13487
Buthus occitanus paris	KTx	P0DL45
Buthus occitanus paris	KTx	P0DL46
Androctonus bicolor	KTx	A0A0K0LCI3
Buthus israelis	KTx	B8XH42
Mesobuthus gibbosus	KTx	B3EWY1
Mesobuthus eupeus	KTx	A0A088DAC3
Mesobuthus eupeus	KTx	D3JXM1
Mesobuthus eupeus	KTx	A0A088D9P9
Mesobuthus eupeus	KTx	A0A088DAY7
Leiurus hebraeus	KTx	P45660
Hottentotta tamulus	KTx	P0C173
Mesobuthus martensii	KTx	Q8MQL0
Mesobuthus martensii	KTx	Q9NBG9
Mesobuthus martensii	KTx	V9LLQ7
Pandinus cavimanus	KTx	H2CYS1
Hemiscorpius lepturus	KTx	A0A1L4BJ36
Hemiscorpius lepturus	KTx	A0A1L4BJ31
Opisthacanthus madagascariensis	KTx	P0C194

Megacormus gertschi	KTx	A0A224XGD9
Anuroctonus phaiodactylus	KTx	P0C166
Superstitionia donensis	KTx	A0A1V1WBW9
Superstitionia donensis	KTx	A0A1V1WBN8
Superstitionia donensis	KTx	A0A1V1WBP1
Hadogenes troglodytes	KTx	A0A1B3IJ17
Scorpiops tibetanus	KTx	P0DP36
Vaejovis smithi	KTx	P0DJ31
Megacormus gertschi	KTx	A0A224X3K8
Vaejovis smithi	KTx	P0DJ32
Hadrurus spadix	KTx	A0A1W7RB29
Hadrurus spadix	KTx	A0A1W7RB38
Hadrurus spadix	KTx	A0A1W7RB23
Hoffmannihadrurus gertschi	KTx	P84864
Hadrurus spadix	KTx	A0A1W7RB41
Hadrurus spadix	KTx	A0A1W7RB24
Hadrurus spadix	KTx	A0A1W7RB16
Hadrurus spadix	KTx	A0A1W7RB43
Opisthacanthus cayaporum	KTx	P86115
Opisthacanthus cayaporum	KTx	P86116
Urodacus yaschenkoi	KTx	A0A0A0PI37
Pandinus imperator	KTx	P55927
Pandinus imperator	KTx	P55928
Urodacus yaschenkoi	KTx	A0A0A0PP73
Urodacus yaschenkoi	KTx	P0DL37
Urodacus yaschenkoi	KTx	A0A0A0PK31
Urodacus yaschenkoi	KTx	A0A0A0PJX6
Urodacus yaschenkoi	KTx	A0A0A0PTG7
Opistophthalmus carinatus	KTx	Q6XLL5
Opistophthalmus carinatus	KTx	Q6XLL6
Opistophthalmus carinatus	KTx	Q6XLL7
Opistophthalmus carinatus	KTx	Q6XLL8
Opistophthalmus carinatus	KTx	Q6XLL9
Heterometrus laoticus	KTx	I6NXS5
Heterometrus spinifer	KTx	P59867
Heterometrus laoticus	KTx	I6NWV2
Opisthacanthus cayaporum	KTx	P86106
Hemiscorpius lepturus	KTx	A0A1L4BJ37
Hemiscorpius lepturus	KTx	P85528
Scorpio palmatus	KTx	P80719

Pandinus imperator	KTx	P58490
Heterometrus spinifer	KTx	P84094
Pandinus imperator	KTx	Q10726
Pandinus imperator	KTx	P58498
Megacormus gertschi	KTx	A0A224XBG0
Superstitionia donensis	KTx	A0A1V1WBN3
Superstitionia donensis	KTx	A0A1V1WC28
Superstitionia donensis	KTx	A0A1V1WBQ0
Superstitionia donensis	KTx	A0A1V1WC84
Lychas mucronatus	NaTx	P0DJ46
Lychas mucronatus	NaTx	P0DJ45
Lychas mucronatus	NaTx	P0DJ48
Mesobuthus martensii	NaTx	P0DJ49
Mesobuthus martensii	NaTx	P0DJ47
Hoffmannihadrurus gertschi	NaTx	P0C8W3
Mesobuthus martensii	NaTx	P0DJ50
Hottentotta tamulus	NaTx	P60277
Hottentotta judaicus	NaTx	F1CJ92
Odontobuthus doriae	NaTx	P84646
Buthacus macrocentrus	NaTx	P0DJH8
Leiurus quinquestriatus	NaTx	P01489
Leiurus hebraeus	NaTx	P83644
Buthus israelis	NaTx	B8XGX9
Hottentotta tamulus	NaTx	P84614
Androctonus bicolor	NaTx	A0A0K0LBX2
Mesobuthus eupeus	NaTx	P86403
Mesobuthus eupeus	NaTx	D8UWD8
Mesobuthus eupeus	NaTx	A0A146CJ08
Mesobuthus eupeus	NaTx	P09982
Buthus israelis	NaTx	B8XGY7
Buthus israelis	NaTx	B8XGY1
Hottentotta judaicus	NaTx	D5HR55
Hottentotta judaicus	NaTx	F0V3W1
Hottentotta judaicus	NaTx	Q56TT9
Hottentotta judaicus	NaTx	F1CJ53
Hottentotta judaicus	NaTx	F0V3W0
Mesobuthus eupeus	NaTx	A0A146CJC0
Hottentotta judaicus	NaTx	F1CJ49
Mesobuthus martensii	NaTx	P0DMH9
Mesobuthus martensii	NaTx	P56569

Mesobuthus martensii	NaTx	P59853	
Mesobuthus martensii	NaTx	P54135	
Mesobuthus martensii	NaTx	Q86BW9	
Androctonus bicolor	NaTx	D5HR49	
Androctonus mauritanicus	NaTx	Q2YHM1	
Androctonus amoreuxi	NaTx	Q86SE0	
Buthus israelis	NaTx	B8XGY3	
Buthus israelis	NaTx	B8XGZ6	
Mesobuthus eupeus	NaTx	A0A0B5GD34	
Mesobuthus martensii	NaTx	G4V3T9	
Mesobuthus martensii	NaTx	A0F0C1	
Mesobuthus martensii	NaTx	Q9NJC7	
Mesobuthus martensii	NaTx	Q9GNG8	
Mesobuthus martensii	NaTx	Q49S27	
Mesobuthus martensii	NaTx	Q9GYX2	
Mesobuthus martensii	NaTx	Q95P69	
Mesobuthus martensii	NaTx	Q1EG63	
Mesobuthus martensii	NaTx	Q4TUA4	
Mesobuthus martensii	NaTx	Q9GUA7	
Mesobuthus eupeus	NaTx	A0A143FHE4	
Mesobuthus martensii	NaTx	P82815	
Mesobuthus eupeus	NaTx	D8UWD3	
Mesobuthus eupeus	**NaTx**	**P86408***	[1]
Mesobuthus eupeus	NaTx	P01490	
Androctonus australis	NaTx	Q9BLM4	
Androctonus mauritanicus	NaTx	P01482	
Leiurus quinquestriatus	**NaTx**	**P01481***	[2-5]
Androctonus crassicauda	NaTx	M1JMR8	
Buthus tunetanus	NaTx	P01486	
Androctonus bicolor	NaTx	D5HR48	
Androctonus mauritanicus	**NaTx**	**Q7YXD3***	[2] [4]
Androctonus crassicauda	NaTx	D5HR52	
Androctonus crassicauda	NaTx	D5HR51	
Buthus israelis	NaTx	B8XGY5	
Buthus tunetanus	**NaTx**	**P01485***	[6]
Leiurus hebraeus	NaTx	D5HR56	
Androctonus australis	**NaTx**	**P01484***	[2-5]
Leiurus hebraeus	**NaTx**	**P59355***	[7-8]
Odontobuthus doriae	NaTx	A0A4D6P363	
Buthus occitanus mardochei	NaTx	P60258	

Buthus occitanus mardochei	NaTx	P60256
Buthus occitanus mardochei	NaTx	P60255
Buthus occitanus mardochei	NaTx	P60259
Odontobuthus doriae	NaTx	A0A0U4RZC4
Androctonus bicolor	NaTx	A0A0K0LBU4
Mesobuthus martensii	NaTx	Q9GQW3
Mesobuthus martensii	NaTx	Q1EG64
Mesobuthus martensii	NaTx	Q1EG65
Hadrurus spadix	NaTx	A0A1W7R9B4
Buthus israelis	NaTx	B8XGY0
Buthus israelis	NaTx	B8XGY9
Androctonus crassicauda	NaTx	M1JB54
Androctonus garzonii	NaTx	E6ZB76
Androctonus bicolor	NaTx	A0A0K0LBW7
Androctonus mauritanicus	NaTx	D5HR54
Androctonus amoreuxi	NaTx	Q86SD9
Buthus israelis	NaTx	B8XGZ5
Buthus israelis	NaTx	B8XGY8
Buthus israelis	NaTx	B8XGZ2
Buthus tunetanus	NaTx	Q17254
Odontobuthus doriae	NaTx	A0A0U4Q545
Leiurus hebraeus	NaTx	D5HR57
Buthus occitanus mardochei	NaTx	P13488
Leiurus hebraeus	NaTx	P56678
Leiurus hebraeus	NaTx	P59357
Mesobuthus eupeus	NaTx	E7CZZ1
Mesobuthus eupeus	NaTx	A0A146CJ90
Buthus tunetanus	NaTx	P01483
Buthus occitanus mardochei	NaTx	P59896
Buthus tunetanus	NaTx	P01488
Buthus occitanus mardochei	NaTx	P59354
Mesobuthus eupeus	NaTx	P09981
Mesobuthus eupeus	NaTx	G4WFQ2
Mesobuthus eupeus	NaTx	E7CZY9
Mesobuthus eupeus	NaTx	E7CZZ0
Mesobuthus eupeus	NaTx	D8UWD5
Mesobuthus eupeus	NaTx	D8UWD6
Mesobuthus eupeus	NaTx	E7D082
Mesobuthus eupeus	NaTx	P86404
Mesobuthus eupeus	NaTx	P86405

Mesobuthus martensii	NaTx	P59854	
Mesobuthus martensii	NaTx	Q9NJC5	
Mesobuthus martensii	NaTx	Q9GQV6	
Mesobuthus martensii	NaTx	P45697	
Mesobuthus martensii	NaTx	P59360	
Mesobuthus martensii	NaTx	P58488	
Mesobuthus martensii	NaTx	Q6IZE0	
Mesobuthus martensii	NaTx	P15227	
Mesobuthus martensii	NaTx	P45698	
Mesobuthus martensii	NaTx	Q9N682	
Mesobuthus martensii	NaTx	B6A8R9	
Mesobuthus martensii	NaTx	B6A8S0	
Lychas mucronatus	NaTx	A0A0U1TXT4	
Mesobuthus martensii	NaTx	O61705	
Mesobuthus martensii	NaTx	Q6IZE1	
Mesobuthus martensii	NaTx	P58328	
Mesobuthus martensii	NaTx	Q9NJC8	
Buthus israelis	NaTx	B8XGY4	
Buthus israelis	NaTx	B8XGZ4	
Mesobuthus martensii	NaTx	E7CAU3	
Mesobuthus martensii	NaTx	Q9NJC4	
Buthus occitanus mardochei	NaTx	P60257	
Buthus israelis	NaTx	B8XGY6	
Buthus israelis	NaTx	B8XGZ0	
Buthus tunetanus	NaTx	P55902	
Androctonus australis	NaTx	Q9BLM3	
Leiurus hebraeus	NaTx	P17728	
Leiurus quinquestriatus	NaTx	P01487	
Buthus tunetanus	NaTx	P04099	
Oscrobiculosus	NaTx	P15224	
Androctonus crassicauda	NaTx	D5HR50	
Androctonus australis	**NaTx**	**P01479***	[9]
Androctonus bicolor	NaTx	A0A0K0LBW8	
Androctonus crassicauda	NaTx	M1JBC0	
Lychas mucronatus	NaTx	P0CI55	
Lychas mucronatus	NaTx	A0A0U1SBV9	
Lychas mucronatus	NaTx	D9U298	
Lychas mucronatus	NaTx	P0CI54	
Androctonus crassicauda	NaTx	M1J7U4	
Androctonus crassicauda	NaTx	E7BLC7	

Androctonus australis	NaTx	P80950	
Androctonus australis	NaTx	P56743	
Centruroides hentzi	NaTx	A0A2I9LPB3	
Centruroides hentzi	NaTx	A0A2I9LPC3	
Centruroides hentzi	NaTx	A0A2I9LPB4	
Centruroides hentzi	NaTx	A0A2I9LPC0	
Superstitionia donensis	NaTx	A0A1V1WBP9	
Superstitionia donensis	NaTx	A0A1V1WC92	
Superstitionia donensis	NaTx	A0A1V1WBQ9	
Superstitionia donensis	NaTx	A0A1V1WBQ8	
Aphaiodactylus	NaTx	Q5MJP5	
Urodacus manicatus	NaTx	T1DPA4	
Cercophonius squama	NaTx	T1DEJ4	
Cercophonius squama	NaTx	T1DMR2	
Megacormus gertschi	NaTx	A0A224X3Y8	
Superstitionia donensis	NaTx	A0A1V1WBR1	
Tityus serrulatus	NaTx	A0A218QXD4	
Centruroides exilicauda	NaTx	Q68PG5	
Centruroides exilicauda	NaTx	Q68PG6	
Centruroides sculpturatus	NaTx	P01491	
Centruroides sculpturatus	NaTx	Q6V4Z0	
Centruroides sculpturatus	NaTx	Q6V4Z1	
Centruroides sculpturatus	NaTx	Q95WD3	
Centruroides noxius	NaTx	P15223	
Centruroides noxius	NaTx	Q6V4Z2	
Centruroides noxius	NaTx	P45665	
Centruroides noxius	NaTx	Q6V4Z3	
Centruroides exilicauda	NaTx	Q68PG2	
Centruroides limpidus	NaTx	P59865	
Centruroides exilicauda	NaTx	Q68PG4	
Centruroides exilicauda	NaTx	Q68PG7	
Centruroides limpidus	NaTx	Q7Z1K5	
Centruroides limpidus	NaTx	P45666	
Centruroides noxius	**NaTx**	**Q9TWL0***	[10-11]
Centruroides limpidus	**NaTx**	**C0HK69***	[12]
Centruroides limpidus	NaTx	Q7Z1K9	
Centruroides sculpturatus	NaTx	Q6V4X9	
Centruroides sculpturatus	NaTx	Q95WD2	
Centruroides limpidus	NaTx	Q7Z1K8	
Centruroides noxius	NaTx	Q9TWL1	

Centruroides infamatus	NaTx	P59897	
Centruroides limpidus	NaTx	P59899	
Centruroides elegans	**NaTx**	**P0CH41***	[13]
Centruroides limpidus	**NaTx**	**P59898***	[14]
Centruroides tecomanus	NaTx	P18926	
Centruroides noxius	NaTx	P80076	
Centruroides noxius	**NaTx**	**P45662***	[15-16]
Centruroides sculpturatus	NaTx	P56646	
Centruroides noxius	**NaTx**	**P01495***	[17-18]
Centruroides suffusus	**NaTx**	**P08900***	[19-22]
Centruroides suffusus	**NaTx**	**P60266***	[23-26]
Centruroides suffusus	**NaTx**	**P0DL83***	[21]
Centruroides suffusus	NaTx	P60267	
Centruroides sculpturatus	NaTx	Q95WD1	
Centruroides sculpturatus	NaTx	P58778	
Centruroides limpidus	**NaTx**	**Q8WRY4***	[27]
Centruroides exilicauda	NaTx	Q68PG3	
Centruroides sculpturatus	NaTx	Q95WC9	
Centruroides noxius	NaTx	Q6V4Y2	
Centruroides noxius	NaTx	Q94435	
Centruroides gracilis	NaTx	P60163	
Lychas mucronatus	NaTx	P0CI56	
Lychas mucronatus	NaTx	P0CI57	
Centruroides hentzi	NaTx	A0A2I9LPA7	
Centruroides hentzi	NaTx	A0A2I9LPA8	
Centruroides hentzi	NaTx	A0A2I9LP86	
Centruroides hentzi	NaTx	A0A2I9LPA9	
Centruroides sculpturatus	NaTx	P01494	
Centruroides sculpturatus	NaTx	Q6V4Y9	
Centruroides sculpturatus	NaTx	P01493	
Centruroides noxius	**NaTx**	**P45663***	[28-29]
Centruroides suffusus	NaTx	B7FDP2	
Centruroides noxius	NaTx	Q6V4Y8	
Centruroides noxius	NaTx	P45664	
Centruroides noxius	NaTx	Q6V4Y7	
Centruroides limpidus	NaTx	Q7YT61	
Centruroides limpidus	NaTx	Q7Z1K6	
Centruroides limpidus	**NaTx**	**P45667***	[30-31]
Centruroides limpidus	NaTx	Q7Z1K7	
Centruroides exilicauda	NaTx	Q68PH2	

Centruroides exilicauda	NaTx	Q68PH1	
Centruroides exilicauda	NaTx	Q68PG9	
Centruroides exilicauda	NaTx	Q68PH3	
Centruroides exilicauda	NaTx	Q68PG8	
Centruroides exilicauda	NaTx	Q68PH0	
Centruroides exilicauda	NaTx	Q68PH4	
Centruroides sculpturatus	NaTx	Q6V4Y4	
Centruroides sculpturatus	NaTx	Q6V4Y3	
Centruroides sculpturatus	NaTx	Q6V4Y5	
Centruroides sculpturatus	NaTx	Q6V4Y6	
Centruroides limpidus	NaTx	Q7Z1K4	
Centruroides sculpturatus	NaTx	P01492	
Megacormus gertschi	NaTx	A0A224XF48	
Lychas mucronatus	NaTx	P0CI51	
Lychas mucronatus	NaTx	P0CI53	
Lychas mucronatus	NaTx	D9U2A0	
Isometrus maculatus	NaTx	A0A0U1TZ19	
Lychas mucronatus	NaTx	A0A0U1TXP5	
Lychas mucronatus	NaTx	P0CI52	
Centruroides hentzi	NaTx	A0A2I9LPA5	
Centruroides vittatus	NaTx	F8UWP3	
Centruroides hentzi	NaTx	A0A2I9LPC1	
Centruroides hentzi	NaTx	A0A2I9LPC6	
Centruroides elegans	NaTx	P0CH40	
Tityus obscurus	NaTx	H1ZZH9	
Tityus obscurus	NaTx	A0A1E1WW03	
Tityus discrepans	NaTx	C9X4K6	
Tityus obscurus	NaTx	H1ZZH8	
Tityus pachyurus	NaTx	H1ZZI5	
Tityus stigmurus	NaTx	P0C8X5	
Tityus serrulatus	NaTx	A0A218QX01	
Tityus serrulatus	**NaTx**	**P01496***	[11] [31-35]
Tityus serrulatus	NaTx	A0A218QXH0	
Tityus serrulatus	NaTx	A0A218QWV4	
Tityus serrulatus	NaTx	P46115	
Tityus fasciolatus	NaTx	P0DSO4	
Tityus bahiensis	NaTx	P0C5K8	
Tityus bahiensis	NaTx	A0A0C9RFQ1	
Tityus bahiensis	**NaTx**	**P56608***	[36]
Parabuthus granulatus	NaTx	B7SNV8	

Parabuthus granulatus	NaTx	P0C5F0	
Parabuthus granulatus	NaTx	P0C5F1	
Parabuthus transvaalicus	NaTx	P58910	
Heteroctenus junceus	NaTx	E7CLP0	
Heteroctenus junceus	NaTx	E7CLN9	
Heteroctenus junceus	NaTx	E7CLN7	
Heteroctenus junceus	NaTx	E7CLN8	
Tityus obscurus	NaTx	A0A1E1WVY8	
Tityus obscurus	NaTx	H1ZZI3	
Centruroides sculpturatus	NaTx	P46066	
Centruroides hentzi	NaTx	A0A2I9LP99	
Centruroides hentzi	NaTx	A0A2I9LPB0	
Lychas mucronatus	NaTx	P0CI50	
Lychas mucronatus	NaTx	D9U2A1	
Lychas mucronatus	NaTx	A0A0U1SE96	
Lychas mucronatus	NaTx	A0A0U1SN99	
Lychas mucronatus	NaTx	A0A0U1TYU4	
Lychas mucronatus	NaTx	A0A0U1TZJ1	
Lychas mucronatus	NaTx	P0CI58	
Isometrus maculatus	NaTx	A0A0U1SCE1	
Isometrus maculatus	NaTx	A0A0U1SEW9	
Isometrus maculatus	NaTx	A0A0U1SCD9	
Isometrus maculatus	NaTx	A0A0U1TZ49	
Isometrus maculatus	NaTx	A0A0U1SEX3	
Isometrus maculatus	NaTx	A0A0U1SCE6	
Isometrus maculatus	NaTx	P0DJK8	
Lychas mucronatus	NaTx	A0A0U1SJ71	
Lychas mucronatus	NaTx	A0A0U1S5U0	
Lychas mucronatus	NaTx	D9U297	
Isometrus maculatus	NaTx	A0A0U1TYC2	
Lychas mucronatus	NaTx	P0CI81	
Lychas mucronatus	NaTx	A0A0U1TYI5	
Lychas mucronatus	NaTx	A0A0U1TZH3	
Lychas mucronatus	NaTx	P0CI59	
Lychas mucronatus	NaTx	P0CI60	
Hottentotta judaicus	NaTx	F1CIV2	
Hottentotta judaicus	NaTx	F1CIW7	
Mesobuthus martensii	**NaTx**	**M4GX67***	[37]
Mesobuthus eupeus	NaTx	A0A146CJ61	
Mesobuthus martensii	**NaTx**	**Q9NBW2***	[37-39]

Odontobuthus doriae	NaTx	A0A0U4R446	
Buthus israelis	NaTx	B8XH17	
Androctonus bicolor	NaTx	A0A0K0LBU9	
Androctonus bicolor	NaTx	A0A0K0LBX4	
Mesobuthus eupeus	NaTx	E4VP15	
Hottentotta judaicus	NaTx	F1CIV8	
Leiurus hebraeus	**NaTx**	**P0C5H3***	[40]
Mesobuthus martensii	NaTx	Q9UAC8	
Mesobuthus eupeus	NaTx	P86406	
Mesobuthus eupeus	NaTx	E4VP18	
Mesobuthus eupeus	NaTx	R4H564	
Mesobuthus eupeus	NaTx	F6K6F3	
Mesobuthus martensii	NaTx	Q9UAC9	
Mesobuthus eupeus	NaTx	R4H5E1	
Androctonus bicolor	NaTx	A0A0K0LBV3	
Androctonus mauritanicus	**NaTx**	**P0DPT3***	[41]
Mesobuthus eupeus	NaTx	A0A146CIX0	
Centruroides suffusus	NaTx	F1CGT6	
Centruroides hentzi	NaTx	A0A2I9LPA0	
Centruroides hentzi	NaTx	A0A2I9LPA3	
Centruroides hentzi	NaTx	A0A2I9LP93	
Centruroides hentzi	NaTx	A0A2I9LP94	
Centruroides hentzi	NaTx	A0A2I9LP90	
Centruroides noxius	NaTx	P58296	
Tityus pachyurus	NaTx	H1ZZI8	
Tityus obscurus	NaTx	H1ZZI4	
Tityus discrepans	NaTx	C9X4K4	
Tityus zulianus	NaTx	Q1I165	
Tityus obscurus	NaTx	A0A1E1WVU6	
Tityus obscurus	NaTx	P84693	
Tityus discrepans	NaTx	C9X4J9	
Tityus discrepans	NaTx	C9X4K0	
Tityus discrepans	NaTx	C9X4K1	
Tityus discrepans	NaTx	P0C1X7	
Tityus discrepans	NaTx	C9X4K3	
Tityus discrepans	NaTx	P0CF39	
Tityus serrulatus	NaTx	O77463	
Tityus costatus	NaTx	Q5G8A8	
Tityus fasciolatus	NaTx	P83435	
Tityus fasciolatus	NaTx	P0DQH6	

Tityus bahiensis	NaTx	A0A0C9S394	
Tityus bahiensis	NaTx	P60275	
Tityus obscurus	NaTx	H1ZZI1	
Tityus bahiensis	NaTx	A0A0C9QKU0	
Tityus bahiensis	NaTx	P60276	
Tityus fasciolatus	NaTx	A0A098CLT3	
Tityus fasciolatus	NaTx	C0HJM9	
Tityus bahiensis	NaTx	P56609	
Tityus serrulatus	NaTx	A0A218QWV5	
Tityus serrulatus	NaTx	P68410	
Tityus stigmurus	NaTx	P68411	
Tityus clathratus	NaTx	J9PIJ6	
Tityus stigmurus	NaTx	P56612	
Tityus bahiensis	NaTx	A0A0C9QKV7	
Tityus fasciolatus	NaTx	P0DQH5	
Tityus bahiensis	NaTx	P56611	
Tityus bahiensis	NaTx	A0A0C9RFN5	
Tityus serrulatus	**NaTx**	**P15226***	[42-46]
Tityus costatus	NaTx	Q5G8B8	
Tityus trivittatus	NaTx	P0DMM8	
Tityus fasciolatus	NaTx	P0DSO5	
Tityus clathratus	NaTx	J9PJ66	
Tityus obscurus	NaTx	A0A1E1WVT2	
Tityus obscurus	NaTx	A0A1E1WWK4	
Tityus obscurus	NaTx	A0A1E1WVW4	
Tityus obscurus	NaTx	H1ZZH7	
Tityus discrepans	NaTx	Q1I176	
Tityus discrepans	NaTx	Q1I180	
Tityus obscurus	NaTx	A0A1E1WWE3	
Tityus obscurus	NaTx	P60212	
Tityus obscurus	NaTx	A0A1E1WVW0	
Tityus obscurus	NaTx	P60215	
Tityus discrepans	NaTx	Q1I173	
Tityus discrepans	NaTx	C9X4J8	
Tityus discrepans	NaTx	Q1I177	
Tityus discrepans	NaTx	Q1I164	
Tityus discrepans	NaTx	Q1I178	
Tityus discrepans	NaTx	Q1I163	
Tityus discrepans	NaTx	Q1I169	
Tityus discrepans	NaTx	Q1I179	

Tityus discrepans	NaTx	Q1I172
Tityus discrepans	NaTx	Q1I167
Tityus discrepans	NaTx	P0CF37
Tityus discrepans	NaTx	Q1I174
Tityus zulianus	NaTx	Q2NME3
Tityus pachyurus	NaTx	P84631
Tityus obscurus	NaTx	A0A1E1WVS8
Tityus obscurus	NaTx	P60214
Tityus obscurus	NaTx	H1ZZI0
Tityus obscurus	NaTx	A0A1E1WVN9
Tityus obscurus	NaTx	P60213
Centruroides sculpturatus	NaTx	P58779
Heteroctenus junceus	NaTx	P86992
Heteroctenus junceus	NaTx	E7CLP3
Heteroctenus junceus	NaTx	E7CLP4
Heteroctenus junceus	NaTx	E7CLP5
Heteroctenus junceus	NaTx	E7CLP2
Heteroctenus junceus	NaTx	E7CLN0
Heteroctenus junceus	NaTx	E7CLN5
Heteroctenus junceus	NaTx	E7CLN6
Heteroctenus junceus	NaTx	E7CLN3
Heteroctenus junceus	NaTx	E7CLN4
Heteroctenus junceus	NaTx	E7CLN2
Heteroctenus junceus	NaTx	E7CLN1
Centruroides hentzi	NaTx	A0A2I9LP97
Centruroides hentzi	NaTx	A0A2I9LPA6
Isometrus maculatus	NaTx	A0A0U1S864
Isometrus maculatus	NaTx	A0A0U1SEV0
Isometrus maculatus	NaTx	A0A0U1TZA2
Isometrus maculatus	NaTx	A0A0U1SCC7
Isometrus maculatus	NaTx	P0DJK9
Buthus tunetanus	NaTx	P59863
Buthus israelis	NaTx	B8XH11
Buthus israelis	NaTx	B8XH07
Androctonus australis	NaTx	P81504
Androctonus crassicauda	NaTx	M1INJ1
Leiurus hebraeus	NaTx	P68725
Isometrus maculatus	NaTx	A0A0U1S623
Odontobuthus doriae	NaTx	A0A0U4PXU5
Buthus israelis	NaTx	B8XH12

Buthus israelis	NaTx	B8XH10
Buthus israelis	NaTx	B8XH16
Buthus israelis	NaTx	B8XH18
Buthus israelis	NaTx	B8XH13
Buthus israelis	NaTx	B8XH20
Buthus israelis	NaTx	B8XH14
Buthus israelis	NaTx	B8XH19
Hottentotta tamulus	NaTx	P82814
Hottentotta tamulus	NaTx	P82812
Hottentotta tamulus	NaTx	P82813
Buthus israelis	NaTx	B8XH08
Orthochirus scrobiculosus	NaTx	O76963
Buthus israelis	NaTx	B8XH09
Buthus tunetanus	NaTx	P59864
Leiurus hebraeus	NaTx	P81240
Leiurus hebraeus	NaTx	P0C5I4
Leiurus hebraeus	NaTx	P0C5I8
Leiurus hebraeus	NaTx	P0C5I9
Leiurus hebraeus	NaTx	P0C5I6
Leiurus hebraeus	NaTx	P0C5I3
Leiurus hebraeus	NaTx	P0C5I5
Leiurus hebraeus	NaTx	P0C5I7
Leiurus hebraeus	NaTx	P0C5J0
Androctonus bicolor	NaTx	A0A0K0LBW5
Androctonus bicolor	NaTx	A0A0K0LBV6
Androctonus bicolor	NaTx	A0A0K0LCI1
Androctonus bicolor	NaTx	A0A0K0LBV0
Androctonus bicolor	NaTx	A0A0K0LBW4
Androctonus bicolor	NaTx	A0A0K0LBW0
Androctonus bicolor	NaTx	A0A0K0LCI0
Odontobuthus doriae	NaTx	A0A0U4QNN2
Mesobuthus eupeus	NaTx	A0A146CIR0
Androctonus bicolor	NaTx	A0A0K0LCH7
Androctonus bicolor	NaTx	A0A0K0LBU8
Androctonus bicolor	NaTx	A0A0K0LBV4
Androctonus bicolor	NaTx	A0A0K0LBT5
Leiurus hebraeus	NaTx	P68726
Leiurus hebraeus	NaTx	Q26292
Hottentotta judaicus	NaTx	F1CJ38
Hottentotta saulcyi	NaTx	Q2NNB8

Hottentotta judaicus	NaTx	F1CIX9	
Hottentotta judaicus	NaTx	P24336	
Buthus tunetanus	NaTx	P55904	
Buthacus arenicola	NaTx	P80962	
Buthus tunetanus	NaTx	P55903	
Buthus israelis	NaTx	B8XH21	
Hottentotta tamulus	NaTx	P82811	
Leiurus quinquestriatus	NaTx	P19855	
Mesobuthus eupeus	NaTx	A0A146CIQ1	
Mesobuthus eupeus	NaTx	A0A146CIT8	
Mesobuthus eupeus	NaTx	A0A146CIU6	
Mesobuthus eupeus	NaTx	A0A146CIV1	
Buthus israelis	NaTx	B8XH15	
Mesobuthus gibbosus	NaTx	A0A059UED5	
Mesobuthus gibbosus	NaTx	A0A059UI27	
Mesobuthus martensii	NaTx	Q86M31	
Mesobuthus martensii	NaTx	Q95WX6	
Mesobuthus martensii	**NaTx**	**Q8I0K7**	[47]
Mesobuthus martensii	NaTx	Q17230	
Mesobuthus martensii	NaTx	Q7Z1E1	
Mesobuthus martensii	NaTx	Q9BKJ0	
Mesobuthus martensii	NaTx	P15228	
Mesobuthus martensii	NaTx	Q8T3T0	
Mesobuthus martensii	**NaTx**	**Q9XY87***	[48]
Mesobuthus martensii	NaTx	Q9BKJ1	
Mesobuthus martensii	NaTx	Q17231	
Mesobuthus martensii	NaTx	A9Q1X9	
Mesobuthus martensii	NaTx	P68727	
Mesobuthus martensii	NaTx	A9Q1Y1	
Mesobuthus martensii	NaTx	A9Q1Y0	
Mesobuthus martensii	NaTx	Q9Y1U3	

References

1. Zhu S., Peigneur S., Gao B., Lu X., Cao C., Tytgat J. 2012. Evolutionary diversification of *Mesobuthus* alpha-scorpion toxins affecting sodium channels. Mol. Cell. Proteomics 11:M111.012054-M111.012054.
2. Alami M., Vacher H., Bosmans F., Devaux C., Rosso J.-P., Bougis P.E., Tytgat J., Darbon H., Martin-Eauclaire M.-F. 2003. Characterization of Amm VIII from *Androctonus mauretanicus mauretanicus*: a new scorpion toxin that discriminates between neuronal and skeletal sodium channels. Biochem. J. 375:551-560.

3. Legros C., Ceard B., Vacher H., Marchot P., Bougis P.E., Martin-Eauclaire M.-F. 2005. Expression of the standard scorpion alpha-toxin AaH II and AaH II mutants leading to the identification of some key bioactive elements. Biochim. Biophys. Acta 1723:91-99.
4. Abbas N., Gaudioso-Tyzra C., Bonnet C., Gabriac M., Amsalem M., Lonigro A., Padilla F., Crest M., Martin-Eauclaire M.F., Delmas P. 2013. The scorpion toxin Amm VIII induces pain hypersensitivity through gain-of-function of TTX-sensitive Na[+] channels. Pain 154:1204-1215.
5. Clairfeuille T., Cloake A., Infield D.T., Llongueras J.P., Arthur C.P., Li Z.R., Jian Y., Martin-Eauclaire M.F., Bougis P.E., Ciferri C., Ahern C.A., Bosmans F., Hackos D.H., Rohou A., Payandeh J. 2019. Structural basis of alpha-scorpion toxin action on Nav channels. Structural basis of alpha-scorpion toxin action on Nav channels. Science 363.
6. Benkhadir K., Kharrat R., Cestele S., Mosbah A., Rochat H., el Ayeb M., Karoui H. 2004. Molecular cloning and functional expression of the alpha-scorpion toxin BotIII: pivotal role of the C-terminal region for its interaction with voltage-dependent sodium channels. Peptides 25:151-161.
7. Sautiere P., Cestele S., Kopeyan C., Martinage A., Drobecq H., Doljansky Y., Gordon D. 1998. New toxins acting on sodium channels from the scorpion *Leiurus quinquestriatus hebraeus* suggest a clue to mammalian vs insect selectivity. Toxicon 36:1141-1154.
8. Chen H., Gordon D., Heinemann S.H. 2007. Modulation of cloned skeletal muscle sodium channels by the scorpion toxins Lqh II, Lqh III, and Lqh alphaIT. Pflugers Arch. 439:423-432.
9. Bougis P.E., Rochat H., Smith L.A. 1989. Precursors of *Androctonus australis* scorpion neurotoxins. Structures of precursors, processing outcomes, and expression of a functional recombinant toxin II. J. Biol. Chem. 264:19259-19265.
10. Valdivia H.H., Martin B.M., Ramirez A.N., Fletcher P.L. Jr., Possani L.D. 1994. Isolation and pharmacological characterization of four novel Na+ channel-blocking toxins from the scorpion *Centruroides noxius* Hoffmann. J. Biochem. 116:1383-1391.
11. Schiavon E., Pedraza-Escalona M., Gurrola G.B., Olamendi-Portugal T., Corzo G., Wanke E., Possani L.D. 2012. Negative-shift activation, current reduction and resurgent currents induced by beta-toxins from *Centruroides* scorpions in sodium channels. Toxicon 59:283-293.
12. Olamendi-Portugal T., Restano-Cassulini R., Riano-Umbarila L., Becerril B., Possani L.D. 2017. Functional and immuno-reactive characterization of a previously undescribed peptide from the venom of the scorpion *Centruroides limpidus*. Peptides 87:34-40.
13. Vandendriessche T., Olamendi-Portugal T., Zamudio F.Z., Possani L.D., Tytgat J. 2010. Isolation and characterization of two novel scorpion toxins: The alpha-toxin-like CeII8, specific for Na(v)1.7 channels and the classical anti-mammalian CeII9, specific for Na(v)1.4 channels. Toxicon 56:613-623.

14. Dehesa-Davila M., Ramirez A.N., Zamudio F.Z., Gurrola-Briones G., Lievano A., Darszon A., Possani L.D. 1996. Structural and functional comparison of toxins from the venom of the scorpions *Centruroides infamatus infamatus*, *Centruroides limpidus limpidus* and *Centruroides noxius*. Comp. Biochem. Physiol. 113B:331-339.
15. Carbone E., Prestipino G., Franciolini F., Dent M.A.R., Possani L.D. 1984. Selective modification of the squid axon Na currents by *Centruroides noxius* toxin II-10.J. Physiol. 79:179-184.
16. Vazquez A., Becerril B., Martin B.M., Zamudio F.Z., Bolivar F., Possani L.D. 1993. Primary structure determination and cloning of the cDNA encoding toxin 4 of the scorpion *Centruroides noxius* Hoffmann. FEBS Lett. 320:43-46.
17. Vazquez A., Tapia J.V., Eliason W.K., Martin B.M., Lebreton F., Delepierre M., Possani L.D., Becerril B. 1995. Cloning and characterization of the cDNAs encoding Na+ channel-specific toxins 1 and 2 of the scorpion *Centruroides noxius* Hoffmann. Toxicon 33:1161-1170.
18. Zamudio F.Z., Saavedra R., Martin B.M., Gurrola G.B., Herion P., Possani L.D. 1992. Amino acid sequence and immunological characterization with monoclonal antibodies of two toxins from the venom of the scorpion *Centruroides noxius* Hoffmann. Eur. J. Biochem. 204:281-292.
19. Martin M.-F., Garcia Y., Perez L.G., el Ayeb M., Kopeyan C., Bechis G., Jover E., Rochat H. 1987. Purification and chemical and biological characterizations of seven toxins from the Mexican scorpion, *Centruroides suffusus suffusus*. J. Biol. Chem. 262:4452-4459.
20. Estrada G., Garcia B.I., Schiavon E., Ortiz E., Cestele S., Wanke E., Possani L.D., Corzo G. 2007. Four disulfide-bridged scorpion beta neurotoxin CssII: heterologous expression and proper folding in vitro. Biochim. Biophys. Acta 1770:1161-1168.
21. Espino-Solis G.P., Estrada G., Olamendi-Portugal T., Villegas E., Zamudio F., Cestele S., Possani L.D., Corzo G. 2011. Isolation and molecular cloning of beta-neurotoxins from the venom of the scorpion *Centruroides suffusus suffusus*. Toxicon 57:739-746.
22. Saucedo A.L., del Rio-Portilla F., Picco C., Estrada G., Prestipino G., Possani L.D., Delepierre M., Corzo G. 2012. Solution structure of native and recombinant expressed toxin CssII from the venom of the scorpion *Centruroides suffusus suffusus*, and their effects on Nav1.5 sodium channels. Biochim. Biophys. Acta 1824:478-487.
23. Cestele S., Qu Y., Rogers J.C., Rochat H., Scheuer T., Catterall W.A. 1998. Voltage sensor-trapping: enhanced activation of sodium channels by beta-scorpion toxin bound to the S3-S4 loop in domain II. Neuron 21:919-931.
24. Cestele S., Scheuer T., Mantegazza M., Rochat H., Catterall W.A. 2001. Neutralization of gating charges in domain II of the sodium channel alpha subunit enhances voltage-sensor trapping by a beta-scorpion toxin. J. Gen. Physiol. 118:291-302.

25. Cohen L., Karbat I., Gilles N., Ilan N., Benveniste M., Gordon D., Gurevitz M. 2005. Common features in the functional surface of scorpion beta-toxins and elements that confer specificity for insect and mammalian voltage-gated sodium channels. J. Biol. Chem. 280:5045-5053.
26. Karbat I., Turkov M., Cohen L., Kahn R., Gordon D., Gurevitz M., Frolow F. 2007. X-ray structure and mutagenesis of the scorpion depressant toxin LqhIT2 reveals key determinants crucial for activity and anti-insect selectivity. J. Mol. Biol. 366: 586-601.
27. Corona M., Coronas F.V., Merino E., Becerril B., Gutierrez R., Rebolledo-Antunez S., Garcia D.E., Possani L.D. 2003. A novel class of peptide found in scorpion venom with neurodepressant effects in peripheral and central nervous system of the rat. Biochim. Biophys. Acta 1649:58-67.
28. Garcia C., Becerril B., Selisko B., Delepierre M., Possani L.D. 1997. Isolation, characterization and comparison of a novel crustacean toxin with a mammalian toxin from the venom of the scorpion *Centruroides noxius* Hoffmann. Comp. Biochem. Physiol. 116B:315-322.
29. Corzo G., Prochnicka-Chalufour A., Garcia B.I., Possani L.D., Delepierre M. 2009. Solution structure of Cn5, a crustacean toxin found in the venom of the scorpions *Centruroides noxius* and *Centruroides suffusus suffusus*. Biochim. Biophys. Acta 1794:1591-1598.
30. Lebreton F., Delepierre M., Ramirez A.N., Balderas C., Possani L.D. 1994. Primary and NMR three-dimensional structure determination of a novel crustacean toxin from the venom of the scorpion *Centruroides limpidus limpidus* Karsch. Biochemistry 33:11135-11149.
31. Kirsch G.E., Skattebol A., Possani L.D., Brown A.M. 1989. Modification of Na channel gating by an alpha scorpion toxin from *Tityus serrulatus*. J. Gen. Physiol. 93:67-83.
32. Teixeira C.E., Ifa D.R., Corso G., Santagada V., Caliendo G., Antunes E., De Nucci G. 2003. Sequence and structure-activity relationship of a scorpion venom toxin with nitrergic activity in rabbit corpus cavernosum. FASEB J. 17:485-487.
33. Campos F.V., Coronas F.I.V., Beirao P.S.L. 2004. Voltage-dependent displacement of the scorpion toxin Ts3 from sodium channels and its implication on the control of inactivation. Br. J. Pharmacol. 142:1115-1122.
34. Campos F.V., Moreira T.H., Beirao P.S.L., Cruz J.S. 2004. Veratridine modifies the TTX-resistant Na+ channels in rat vagal afferent neurons. Toxicon 43:401-406.
35. Dang B., Kubota T., Mandal K., Correa A.M., Bezanilla F., Kent S.B. 2016. Elucidation of the covalent and tertiary structures of biologically active Ts3 toxin. Angew. Chem. Int. Ed. 55:8639-8642.
36. Becerril B., Corona M., Coronas F.I., Zamudio F.Z., Calderon-Aranda E.S., Fletcher P.L. Jr., Martin B.M., Possani L.D. 1996. Toxic peptides and genes encoding toxin gamma of the Brazilian scorpions *Tityus bahiensis* and *Tityus stigmurus*. Biochem. J. 313:753-760.
37. Nie Y., Zeng X.C., Luo X., Wu S., Zhang L., Cao H., Zhou J., Zhou L. 2012. Tremendous intron length differences of the BmKBT and a novel

BmKBT-like peptide genes provide a mechanical basis for the rapid or constitutive expression of the peptides. Peptides 37:150-156.
38. Ye J.-G., Wang C.-Y., Li Y.-J., Tan Z.-Y., Yan Y.-P., Li C., Chen J., Ji Y.-H. 2000. Purification, cDNA cloning and function assessment of BmK abT, a unique component from the Old World scorpion species. FEBS Lett. 479:136-140.
39. Ji Y.-H., Wang W.-X., Wang Q., Huang Y.-P. 2002. The binding of BmK abT, a unique neurotoxin, to mammal brain and insect Na(+) channels using biosensor. Eur. J. Pharmacol. 454:25-30.
40. Gordon D., Ilan N., Zilberberg N., Gilles N., Urbach D., Cohen L., Karbat I., Froy O., Gaathon A., Kallen R.G., Benveniste M., Gurevitz M. 2003. An 'Old World' scorpion beta-toxin that recognizes both insect and mammalian sodium channels. Eur. J. Biochem. 270:2663-2670.
41. Oukkache N., ElJaoudi R., Chgoury F., Rocha M.T., Sabatier J.M. 2015. Characterization of Am IT, an anti-insect beta-toxin isolated from the venom of scorpion *Androctonus mauretanicus*. Sheng Li Xue Bao 67:295-304.
42. Possani L.D., Martin B.M., Fletcher M.D., Fletcher P.L. Jr. 1991. Discharge effect on pancreatic exocrine secretion produced by toxins purified from *Tityus serrulatus* scorpion venom. J. Biol. Chem. 266:3178-3185.
43. Marcotte P., Chen L.Q., Kallen R.G., Chahine M. 1997. Effects of *Tityus serrulatus* scorpion toxin gamma on voltage-gated Na+ channels. Circ. Res. 80:363-369.
44. Bucaretchi F., Vinagre A.M., Chavez-Olortegui C., Collares E.F. 1999. Effect of toxin-g from *Tityus serrulatus* scorpion venom on gastric emptying in rats. Braz. J. Med. Biol. Res. 32:431-434.
45. Campos F.V., Chanda B., Beirao P.S., Bezanilla F. 2007. Beta-scorpion toxin modifies gating transitions in all four voltage sensors of the sodium channel. J. Gen. Physiol. 130:257-268.
46. Coelho V.A., Cremonez C.M., Anjolette F.A., Aguiar J.F., Varanda W.A., Arantes E.C. 2014. Functional and structural study comparing the C-terminal amidated beta-neurotoxin Ts1 with its isoform Ts1-G isolated from *Tityus serrulatus* venom. Toxicon 83C:15-21.
47. Peng F., Zeng X.-C., He X.-H., Pu J., Li W.-X., Zhu Z.-H., Liu H. 2002. Molecular cloning and functional expression of a gene encoding an antiarrhythmia peptide derived from the scorpion toxin. Eur. J. Biochem. 269:4468-4475.
48. Guan R.-J., Wang C.-G., Wang M., Wang D.-C. 2001. A depressant insect toxin with a novel analgesic effect from scorpion *Buthus martensii* Karsch. Biochim. Biophys. Acta 1549:9-18.